THE JOURNAL OF PHYSICAL CHEMISTRY A
A JOURNAL OF THE AMERICAN CHEMICAL SOCIETY

pubs.acs.org/JPCA Article

Screening for New Pathways in Atmospheric Oxidation Chemistry with Automated Mechanism Generation

Victoria P. Barber,* William H. Green, and Jesse H. Kroll

Cite This: J. Phys. Chem. A 2021, 125, 6772–6788 Read Online

ABSTRACT: In the Earth's atmosphere, reactive organic carbon undergoes oxidation via a highly complex, multigeneration process, with implications for air quality and climate. Decades of experimental and theoretical studies, primarily on the reactions of hydrocarbons, have led to a canonical understanding of how gas-phase oxidation of organic compounds takes place. Recent research has brought to light a number of examples where the presence of certain functional groups opens up reaction pathways for key radical intermediates, including alkyl radicals, alkoxy radicals, and peroxy radicals, that are substantially different from traditional oxidation mechanisms. These discoveries highlight the need for methods that systematically explore the chemistry of complex, functionalized molecules without being prohibitively expensive. In this work, automated reaction network generation is used as a screening tool for new pathways in atmospheric oxidation chemistry. The reaction mechanism generator (RMG) is used to generate reaction networks for the OH-initiated oxidation of 200 mono- and bifunctionally substituted *n*-pentanes. The resulting networks are then filtered to highlight the reactions of key radical intermediates that are fast enough to compete with traditional atmospheric removal processes as well as "uncanonical" processes which differ from traditionally accepted oxidation mechanisms. Several recently reported, uncanonical atmospheric mechanisms appear in the RMG dataset. These "proof of concept" results provide confidence in this approach as a tool in the search for overlooked atmospheric oxidation chemistry. Several previously unreported reaction types are also encountered in the dataset. The most potentially atmospherically important of these is a radical−carbonyl ring-closure reaction that produces a highly functionalized cyclic alkoxy radical. This pathway is proposed as a promising target for further study via experiments and more detailed theoretical calculations. The approach presented herein represents a new way to efficiently explore atmospheric chemical space and unearth overlooked reaction steps in atmospheric oxidation.

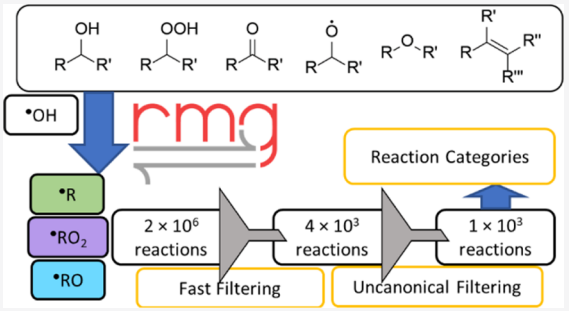

1. INTRODUCTION

Reactive organic carbon (ROC, defined as all organic species excluding methane) is emitted into the troposphere from both natural sources including terrestrial vegetation and biomass burning[1] and anthropogenic sources such as fossil fuel use.[2,3] Upon emission, most primary ROC species undergo oxidation via a highly complex, multigenerational process. This can lead to a wide variety of secondary organic species, with oxidation of a single organic precursor forming thousands of products.[4] As a result, the full ensemble of gas-phase reactive organic species in the atmosphere represents a large and highly complex chemical space[5] involving hundreds of thousands of individual chemical species that differ in both their carbon skeletons and their functional groups.

The oxidation of ROC is central to a number of key atmospheric processes that have implications for climate and human health. It governs radical cycling in the atmosphere and is therefore key in determining total atmospheric reactivity.[6] It dominates the production of tropospheric ozone (O_3), an air pollutant that is detrimental to human health and plant life,[7,8] and controls the degradation and formation of toxic organic species.[9] Further, the chemical changes that result from oxidation lead to corresponding changes in volatility and result in the formation of secondary organic aerosol (SOA), a major component of atmospheric particulate matter,[10] which can have critical impacts on climate[11,12] and human health.[13]

Based on decades of experimental and theoretical research, we have a canonical understanding of how gas-phase oxidation of volatile organic compounds (VOCs) takes place.[6,14,15] In the daytime, oxidation is primarily initiated by the hydroxyl radical (OH) or ozone (O_3), while at night, oxidants include O_3 and nitrate radicals (NO_3). Herein, we focus on OH-initiated oxidation, shown schematically in Figure 1. In this canonical scheme, OH either abstracts a hydrogen atom or

Received: May 14, 2021
Revised: July 20, 2021
Published: August 4, 2021

https://doi.org/10.1021/acs.jpca.1c04297
J. Phys. Chem. A 2021, 125, 6772–6788

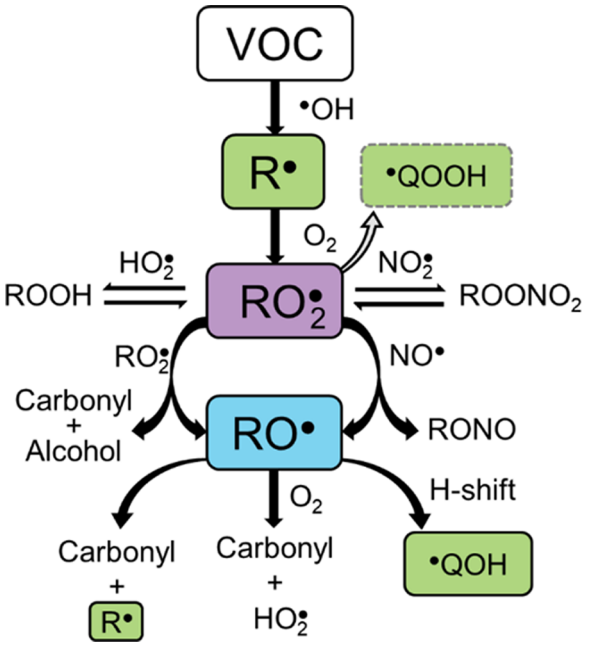

Figure 1. Canonical mechanism for the OH-initiated oxidation of a typical VOC in the troposphere, with a focus on the fates of the key organic radical intermediates along the reaction path: alkyl radicals (R, green), peroxy radicals (RO_2, purple), and alkoxy radicals (RO, blue). The QOOH formation pathway represents a recently appreciated mechanism that now ought to be considered part of the canonical atmospheric oxidation chemistry.

adds to a double bond, leading to an alkyl radical (R). This R radical then reacts rapidly with O_2 to yield a peroxy radical (RO_2). The RO_2 radical has traditionally been assumed to react bimolecularly with other trace atmospheric species to either give closed-shell products that can undergo further oxidation or an alkoxy radical (RO), which can then undergo a unimolecular reaction that leads to chain propagation or form additional closed-shell products.[6,14−16]

This general understanding of the oxidation scheme of organics and the key radical intermediates involved (R, RO_2, and RO) has been developed via investigations of either prototypical VOCs (i.e., simple alkanes and alkenes) or single, particularly abundant atmospheric species (i.e., isoprene or monoterpenes). Structure−activity relationships (SARs) are then typically used to explore the effects of different substituents and carbon skeletons on a given reaction type and are benchmarked against experimental results when available.[17,18] However, this standard description of oxidation chemistry is unlikely to be representative of all organic species in the atmosphere. In particular, most oxidation mechanisms are based on hydrocarbon chemistry, which is most representative of primary ROC. However, far less is known about the chemistry of secondary organic species, which often include a variety of oxygenated functional groups. Beyond just altering relative rates and branching ratios of traditional chemical processes (effects which can be described via SARs), functional groups may open whole new pathways outside of canonical oxidation chemistry. Recent work has brought to light a number of examples of "uncanonical" reaction mechanisms involving the key radical intermediates encountered in OH-initiated oxidation (R, RO, and RO_2) that play an important role in atmospheric organic chemistry and in particular in the production of SOA. We use the term "uncanonical" to refer to reaction mechanisms that are outside of traditional atmospheric VOC oxidation schemes. (This term avoids confusion with the traditional thermodynamics implications of the term "non-canonical".) Perhaps the quintessential example of such a mechanism is the RO_2 radical intramolecular hydrogen atom shift, the key step in the pathway often referred to as "autoxidation". The isomerization reaction forms an alkyl-centered radical with a hydroperoxide functionality (QOOH), to which molecular oxygen then rapidly attaches to form a new, more oxidized RO_2 radical.[19−21] Similar processes have long been known to be important in a variety of different systems, including low-temperature combustion[22] and food spoilage,[23−25] but such chemistry was largely assumed to be unimportant in the context of atmospheric chemistry because, for unfunctionalized RO_2 radicals, the intramolecular H-atom shift is too slow to compete with RO_2 reactions with NO and HO_2.[26−28]

However, recently, it has been shown that the oxidation of some VOCs, such as monoterpenes, can lead to the rapid generation of large amounts of low-volatility products via this mechanism.[29−32] The key to this chemistry is the dramatic enhancement of the H-atom shift rate constant in the presence of particular substituents, an effect initially encountered in computational investigations[33−35] and subsequently measured for substituted RO_2 radicals encountered in the OH-initiated oxidation of isoprene[36] and then for the model system 3-pentanone.[19] Subsequent work has shown that with certain functional groups in particular positions, the greatly accelerated RO_2 H-atom shift can compete with and even dominate over bimolecular reactions, particularly under conditions where concentrations of NO and HO_2 are low, such as in remote or forested environments.[20,37−40] In fact, it is likely that this mechanism is ubiquitous in the atmosphere. For example, it has recently been shown that at least 30% of all isoprene (the most abundantly emitted biogenic VOC)[1,41] will undergo at least one RO_2 H-atom shift during its oxidation.[42] Thus, the RO_2 H-atom shift reaction ought to be incorporated into our canonical understanding of gas-phase atmospheric oxidation chemistry. Though the quantification of the RO_2 radical isomerization pathway's atmospheric impact continues to be a challenge, it is now understood that the highly functionalized, low-volatility products of the autoxidation mechanism make an important contribution to new particle formation and total OA mass.[29−32] The autoxidation mechanism is an example of a pathway that is not available (or, at least, is extremely minor) for simple hydrocarbon species but can be important (or even dominant) for more complex, functionalized molecules.[20,39]

Another such example is the epoxide formation reaction of β-hydroperoxy-substituted R radicals. Again, this pathway requires the presence of a particular functionality (in this case, a hydroperoxy group) in order to be available and is not possible for simple hydrocarbon species. This pathway first gained attention due to the observation of an epoxide (isoprene epoxydiol, IEPOX) as a major product in the OH-initiated oxidation of isoprene[1,41] under low-NO_x conditions.[43] The accepted mechanism for its formation involves the concerted OH loss and ring-closure reaction of a β-hydroperoxy R radical, formed by OH addition to an isoprene hydroxyl hydroperoxide,[43,44] a process which is enhanced due to chemical activation.[45] This pathway dominates the fate of the β-hydroperoxy R radical; more than 80% of the β-hydroperoxy R radicals go on to form IEPOX products, while the remaining fraction undergoes the typical O_2 addition

https://doi.org/10.1021/acs.jpca.1c04297
J. Phys. Chem. A 2021, 125, 6772−6788

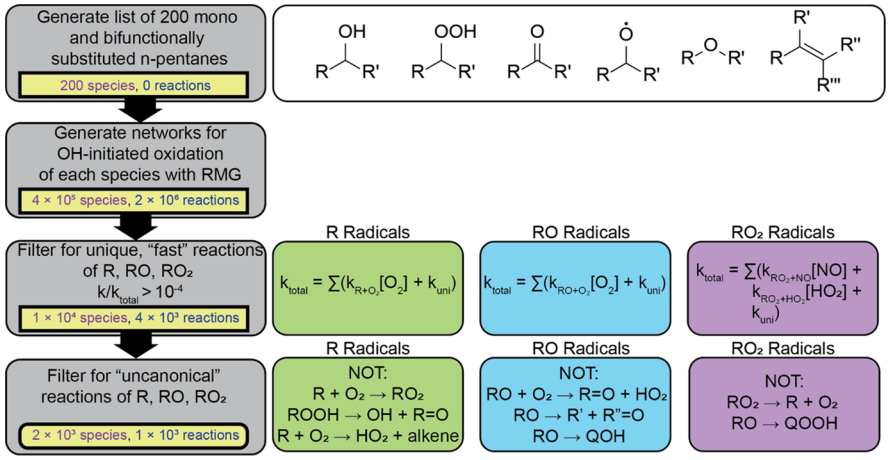

Figure 2. Schematic representation of the generation of the reaction datasets used in this work. Functional groups considered in the initial molecule dataset are shown, as well as basic rules for the two filtering algorithms. The initial network generation step results in ~10^6 reactions, some of which are duplicates. These duplicate reactions are removed during the "fast" filtering step.

pathway to yield a substituted RO_2 radical.[43,45] IEPOX is highly water-soluble, favoring its partitioning into the aerosol phase, and highly reactive, leading to multiphase chemistry that ultimately transforms it into even lower-volatility and more soluble products such as organosulfates, 2-methyltetrols, and oligomers, all of which contribute to SOA.[46−49] Further investigations of the epoxide formation pathway have shown that this chemistry is not limited to isoprene or even to chemically activated systems; with the presence of additional functional groups (in particular, alcohol substituents), energy barriers to epoxide formation are significantly lower,[50,51] suggesting that this pathway could be important for a variety of atmospheric systems.

The discoveries discussed above, in which key radical intermediate species react via pathways that are different from that of canonical chemistry, highlight the need for approaches that move beyond the reactions typically considered for prototypical atmospheric organic species and more thoroughly explore the chemistry of complex, functionalized molecules. In the presence of particular combinations of substituents, it seems likely that there are other uncanonical reaction mechanisms of organic radicals that have been overlooked in atmospheric gas-phase oxidation chemistry. However, the complete set of gas-phase organic compounds (and their associated radical intermediates) in the atmosphere represents an extremely large and complex set of species; exploring the full complexity of atmospheric organic chemistry via experiments is out of the question, and quantum mechanical calculations covering all possible species and reactions are prohibitively expensive. There is a need for methods that can more thoroughly explore this complex chemical space, systematizing the search for potentially important new gas-phase organic oxidation chemistry.

Automated reaction network exploration methods are promising tools for this task. Such methods, which encompass a variety of different algorithmic approaches, are designed to locate intermediates and reaction paths for chemical processes with as little guidance from the user as possible, reducing the role of "chemical intuition" in the pursuit of mechanistic understanding into complex chemical processes.[52−54] Here, automated reaction network exploration is used as a screening tool to investigate the OH-initiated oxidation of a set of substituted *n*-pentanes, representing a simple and well-defined yet relatively broad portion of atmospherically relevant chemical space.

A filtering algorithm is applied to the set of automatically generated reaction networks in order to first identify reactions of key radical intermediates (R, RO, and RO_2) that are fast enough to be of atmospheric importance and then highlight reactions that are "uncanonical", that is, those not typically included in atmospheric oxidation mechanisms. This approach identifies and provides insights into several recently reported, uncanonical atmospheric oxidation mechanisms, including those discussed above, lending confidence to its ability to find such unexpected chemistry. In addition to these recently reported mechanisms, the dataset provides evidence of several reaction classes that have not been previously considered in atmospheric oxidation chemistry. The most notable of these is a carbonyl-substituted radical ring-closing reaction, an important target for further study. More generally, the results demonstrate the importance and utility of methods that can scan large swaths of chemical space in understanding gas-phase organic oxidation in the atmosphere.

2. METHODS

The reaction network exploration is undertaken using the reaction mechanism generator (RMG, rmg.mit.edu, version 3.0.0, accessed March 17, 2020).[55,56] RMG is an open-source, Python-based program which uses an extensive database of kinetic and thermodynamic data, as well as estimation protocols for thermodynamic and kinetic parameters, to automatically generate reaction networks at a relatively low computational cost.

Traditionally, an SAR describes a single prescribed reaction class, involving a well-defined set of reactants and products. Kinetics are then estimated based on relationships derived for this specific reaction from sets of theoretical data, usually benchmarked to experimental results. The RMG approach is somewhat different; rather than following prescribed rules for how particular intermediate types react, it relies on highly generalized reaction templates, making it more flexible and more likely to find previously unexplored chemistry.

RMG is developed for and typically applied to combustion systems, but given the similarity between atmospheric organic oxidation chemistry and low-temperature combustion (the atmosphere is sometimes described as a "low-temperature

https://doi.org/10.1021/acs.jpca.1c04297
J. Phys. Chem. A 2021, 125, 6772−6788

flame"), it is also highly applicable to atmospheric systems. However, there are a number of limitations associated with applying RMG to atmospheric systems. Most notably, at atmospherically relevant temperatures, small uncertainties in reaction barrier heights lead to much larger uncertainties in rates, as compared to those at higher temperatures. Hence, the uncertainties associated with rates and branching ratios in RMG-predicted networks at atmospheric temperatures can be quite large. Therefore, in this work, rather than generating quantitative models of the oxidation of single, atmospherically relevant species, RMG is used as a screening tool, which allows for the scanning of a large portion of chemical space in a short time and with a relatively low computational cost.

RMG is used to generate reaction networks for the OH-initiated oxidation of a set of 200 mono- and bifunctionally substituted *n*-pentanes with atmospherically relevant functional groups. The resulting dataset of reactions is combined and then filtered to create two datasets. The first is a set of "fast" reactions—reactions that have high enough rate constants to represent significant removal processes under atmospheric conditions. The second is a set of uncanonical reactions—reactions that are not typical of atmospheric gas-phase organic oxidation schemes. The process for generating these reaction sets is shown schematically in Figure 2.

2.1. RMG Reaction Network Generation. Six functional groups are considered in defining the initial set of oxidized molecules, including alcohols, hydroperoxides, carbonyls, alkoxy radicals, ethers, and alkenes, as shown in Figure 2. Ethers and alkenes are incorporated into the *n*-pentane skeleton. RO_2 + NO reactions are generally not of major importance in combustion chemistry and are thus not well-parameterized in RMG. Therefore, rather than including NO_x chemistry that would convert peroxy radicals to alkoxy radicals under atmospheric conditions, alkoxy radicals are included as a starting functional group. All chemically reasonable (i.e., not exceeding four bonds to carbon atoms) mono- and bifunctional substitution patterns of the *n*-pentane skeleton are considered for each combination of these functional groups, resulting in a set of 200 organic compounds. Because alkoxy radicals are included as a starting functional group, only unfunctionalized and monofunctional alkoxy radicals (for a total of 55 RO radicals) are included in the dataset (no biradicals are considered). This limits the potential for this work to discover uncanonical alkoxy chemistry. For example, the dataset herein does not include any examples of a recently reported uncanonical RO radical α-ester rearrangement reaction, which would involve a bifunctional RO radical that is not encountered in the dataset presented here.[57] Future work may explore a more complete inclusion of multifunctional RO radicals. Organic acids, peroxides (apart from hydroperoxides), peroxyacids, and esters are not included as separate functional groups but do appear in the set of organic compounds as combinations of other functional groups (i.e., substitution of the same carbon with an alcohol and carbonyl group is equivalent to an organic acid group, or two consecutive ether substituents is equivalent to a peroxide). A full list of molecules included in the dataset is included in Table S1.

RMG, which is described in detail elsewhere,[55] uses a rate-based algorithm to determine which species and reactions to include in the model. Briefly, the initial species in the user-defined reaction system are placed into the "core" of the model, and RMG determines all possible reactions of the core species, generating a list of all possible product species in the model "edge". Then, the reactor is initialized at time 0 and propagated forward in time until the flux to an edge species exceeds a user-specified tolerance level. At this point, the edge species with the largest flux is brought into the core, and the process is repeated until the model reaches a user-specified termination criterion.

The reaction generation process relies on a set of reaction families, each of which consists of a template that describes the reactive sites, and a "recipe" that defines how bond connectivity changes from reactants to products. 70 reaction families are included in RMG (the full list of reaction families is described elsewhere);[55,56] no additional reaction families are added for the purposes of this work. The families are defined to be quite broad and often do not include specific atoms in their definitions. A reaction must fall within one of the family definitions to be picked up by RMG, and it is possible that this approach may not find all uncanonical reaction pathways, particularly if the reaction type is wholly unknown. Nevertheless, the broad definitions of the reaction families allow RMG to search a large swath of chemical space for reaction pathways that may be missed by chemical intuition.

RMG relies on a system of hierarchical trees to estimate kinetics associated with individual reactions.[55,56] One tree is associated with each reaction family and used to estimate kinetics associated with the reactions it generates. Within a single tree, there is a set of child nodes. Nodes that are further down the tree represent more specific and mutually exclusive subdivisions of the reactions. Some nodes of the tree contain rate rule information, populated via the use of "training reactions"—that is, reactions for which detailed quantum mechanical calculations have been performed and rates calculated. Nodes of each tree are filled in where possible using a rate rule from the training reaction that best matches that node. When no training reaction is available for a particular node of the tree, the rate is estimated based on the average of its child nodes. Then, when a mechanism is generated, rates for individual reactions are estimated by descending the trees as far as possible and matching to the rate rules in that tree. If a particular node does not have rate rule information, the program will move up the tree until it finds the nearest parent nodes that contain rate rules and estimate using a geometric average of the rate rules associated with these nodes. In some cases, this node may be the highest node on the tree, for which a rate rule is always defined. This means that the accuracy of predicted rate constants is highly dependent on how densely the rate rules for its associated tree are populated or, in other words, how many different training reactions are available for that tree. The RMG database, which includes all training reactions and definitions of reaction families, is available at rmg.mit.edu/database/. No additional training reactions have been added for the purposes of this work, but additional training reactions can be included, improving the accuracy of the model generation as more data become available.

The parameters used for reaction network generation are briefly summarized here. All networks are generated at a temperature of 298 K and a pressure of 1 bar. Initial mole fractions are given in Table S2. For all closed-shell precursor molecules, the mole fraction of OH is considerably lower than that of the starting VOC. Therefore, closed-shell products do not undergo further oxidation, though radical species may react further. For alkoxy radical precursors, no OH is included in the

https://doi.org/10.1021/acs.jpca.1c04297
J. Phys. Chem. A 2021, 125, 6772−6788

initial reactor because starting from a radical species precludes the need for OH to initiate oxidation. Instead, the alkoxy radical is given an initial concentration equal to the concentration of OH in the other generated networks, avoiding anomalously high radical concentrations. The tolerance for moving a reaction into the model core is set to be 0.02, meaning that the rate at which a species in that reaction is produced must exceed 0.02 times the characteristic rate of the reaction system, R_{char}. R_{char} is defined as the sum of all core species production rates, R_j[55]

$$R_{char} = \sqrt{\sum_j R_j^2}, \text{ species } j \in \text{core} \quad (1)$$

The model is set to terminate after 24 h of model time. In each case, we include first-generation H-atom abstraction and (in the case of alkenes) OH addition products as initial core species with 0 concentration. This forces the program to include these species in the model core; doing so avoids missing entire branches of the reaction network due to incorrectly estimated H-atom abstraction rates. These possible initial H-atom abstraction or OH addition products are determined based on the master chemical mechanisms (MCM) v3.3.1 (http://mcm.leeds.ac.uk/MCM) when precursors are included in the MCM.[58,59] When the closed-shell precursor molecule is not in the MCM, all possible first-generation H-atom abstraction and OH addition products are included as initial core species. Generated species are constrained to have a maximum of two radical electrons and 10 oxygen atoms, though in practice, biradicals are not encountered in the dataset.

While RMG has the capability to generate pressure-dependent reaction networks, which take into account the role of chemical activation in multistep unimolecular reaction pathways,[60] this approach is not used here. Instead, the assumption is made that all reactions occur under thermal conditions. Including chemical activation would make the network generation process more computationally expensive, as well as complicating the filtering process described below. Most of the molecules that appear in the RMG-generated dataset are fairly large (an unsubstituted *n*-pentane has 45 vibrational degrees of freedom, including a number of low-frequency torsional modes) and therefore provide a large reservoir of states for excess internal energy. This reduces the importance of chemical activation except in cases where highly exothermic reaction steps result in a very high degree of internal excitation. As will be discussed throughout this work, the assumption of full thermalization is not necessarily valid for all reaction types, and future work is needed to address how chemical activation can be included more rigorously in the reaction screening process.

The RMG network generation runs are performed using a single processor on a typical PC, without the need for special hardware or computing resources. Most individual network generation runs (for a single species) take on the order of 10 min. Input files, output files, and species dictionaries generated for each RMG run are available in the Supporting Information.

2.2. Reaction Filtering Algorithm. After each reaction network is generated, reactions involving each of the three key radical intermediate types (R, RO, and RO_2) are screened based on whether they are fast enough to compete with other removal processes and then based on whether they are uncanonical. A reaction-by-reaction approach is used, wherein each elementary reaction step is separated from the overall network in which it was generated and then assessed to determine its potential atmospheric importance. From the total set of elementary reaction steps, the radical reactions are filtered according to an algorithm, which is written in Python version 3.7 and makes use of the RMG application programming interface and the RDKit, pandas, and NumPy Python packages.[61−63] The code associated with the filtering algorithm is available in the Supporting Information.

2.2.1. Filtering for Fast Reactions. The filtering for fast reactions is based on thermal rates at a temperature of 298 K and a pressure of 1 atm. The ratio between the rate of a given reaction of a species and the total removal rate of that species (k/k_{total}) must be greater than a "low-cutoff" factor of the total removal rate for the reactant in order to be considered "fast". For training reactions, the uncertainty in rates is often 1 order of magnitude or less, but for reaction rates that are estimated in RMG, the uncertainty can be much greater. In this work, a low-cutoff factor of 10^{-4} is used, which allows for several orders of magnitude of uncertainty in rates without erroneously filtering out potentially important reactions. As noted above, this filtering method does not consider the possible role of chemical activation in enhancing reaction rates/branching ratios. However, using such a low-cutoff factor should also ensure that many reactions that occur primarily due to chemical activation will make it past this fast filtering step.

In order to filter based on this ratio, the total removal rate of each reactant must be determined. This total removal rate takes a different form depending on the reactant radical type. For alkyl and alkoxy radicals (R and RO), we use the sum of all the reaction rates available to that species as predicted by RMG, including pseudo-first-order reaction rates with O_2 (using an O_2 mole fraction of 0.20) and unimolecular reactions. For both of the filtering algorithms, vinoxy radicals [−•CC(═O)−] are treated the same as R radicals, as vinoxy radicals follow the same conventional O_2 addition pathway.[64−66]

For peroxy radicals (RO_2), the chemistry is more complex due to the number of possible bimolecular and unimolecular reactions. While the reactions with NO and HO_2 are not included in the network generation process, any potentially important uncanonical reaction of RO_2 must be competitive with these canonical bimolecular processes. Therefore, these bimolecular reactions are considered in the filtering algorithm. To calculate the total removal rate for an RO_2 radical, we use the sum of all unimolecular reaction rates predicted in RMG and then add pseudo-first-order reaction rates with NO and HO_2. We use 8.5×10^{-12} cm^3 $molecule^{-1}$ s^{-1} for the RO_2 + NO rate constant and 2×10^{-12} cm^3 $molecule^{-1}$ s^{-1} for the RO_2 + HO_2 rate constant.[20,59] Concentrations of NO and HO_2 of 20 and 50 ppt, respectively, are used, corresponding to associated RO_2 lifetimes of 200 and 40 s, respectively. These concentrations are typical for unpolluted forested conditions,[67] an environment in which RO_2 radicals have a long lifetime with respect to the reaction with NO and HO_2, allowing substantial time for unimolecular chemistry to take place. Reactions with other RO_2' radicals may also decrease the lifetime of RO_2 in the atmosphere, but are more difficult to reduce to a single pseudo-first-order rate constant due to the dependence of the RO_2 + RO_2' reaction rate on the structure of the RO_2 radicals in question.[68] These reactions are therefore not included in the filtering process.

https://doi.org/10.1021/acs.jpca.1c04297
J. Phys. Chem. A 2021, 125, 6772−6788

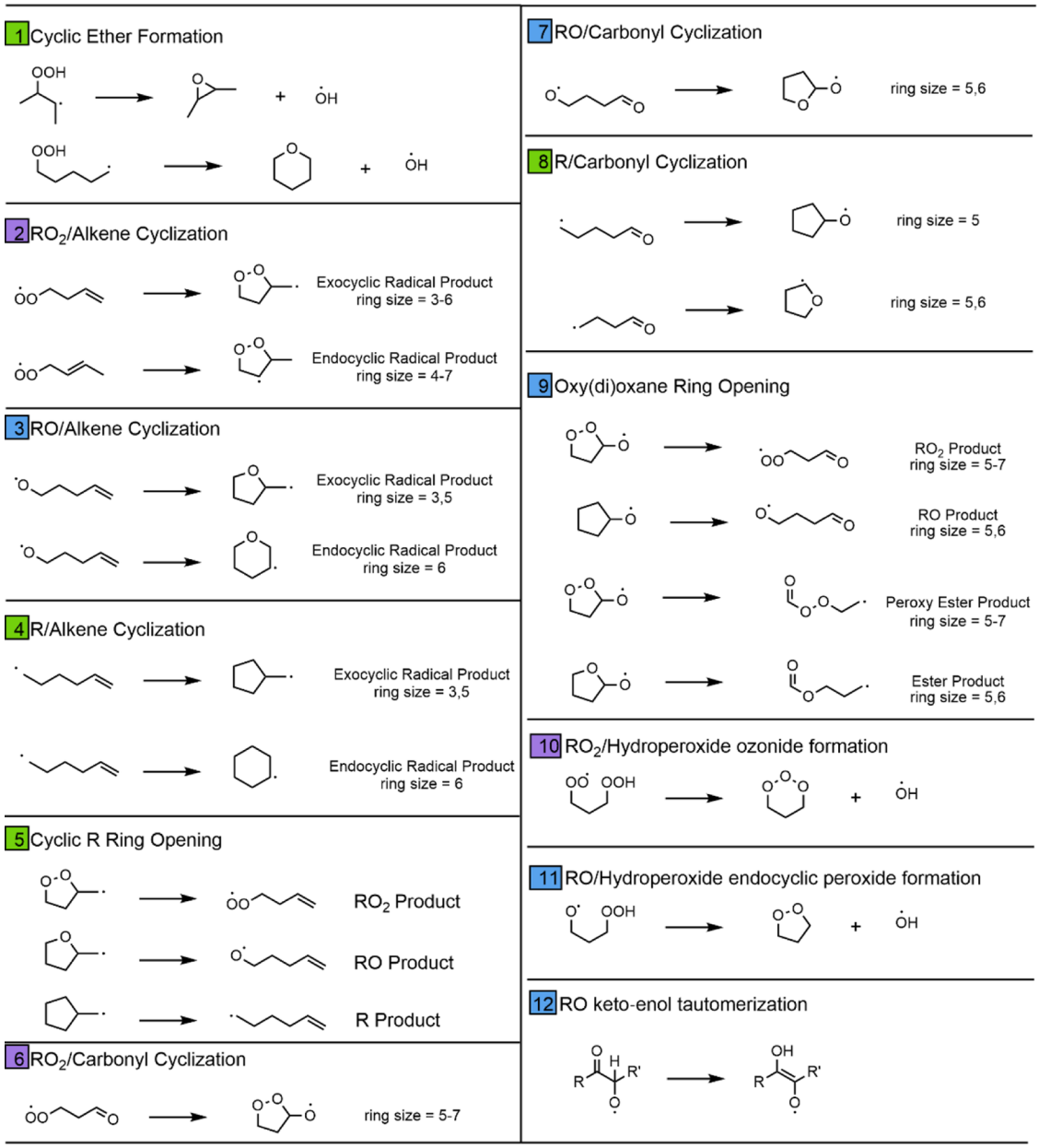

Figure 3. Reaction categories for uncanonical reactions found in the filtered RMG dataset and referred to throughout the text. Reaction numbers are colored according to whether the reactants are R (green), RO (blue), or RO_2 (purple) radicals. Where relevant, the ring sizes listed refer to those sizes encountered in the filtered dataset. In each case, the reaction of interest is shown in the simplest possible terms; additional alkyl and oxygenated substituents are possible in all cases.

2.2.2. Filtering for Uncanonical Reactions. Each of the "fast" reactions is important in understanding the full product distribution resulting from OH-initiated oxidation of a given compound; however, the goal of this work is to identify reaction classes that are outside of canonical oxidation schemes. Hence, the list of "fast" reactions generated from the filtering described above is then filtered again to remove oxidation steps typical of standard oxidation mechanisms, leaving only uncanonical reactions in the resulting dataset. Again, this filtering takes different forms for each radical type.

For R radicals, standard oxidation mechanisms involve O_2 addition to the radical site, and such reactions are filtered out. In cases where the alkyl radical site is located on a carbon atom bearing a hydroperoxide functional group, the understood mechanism is the elimination of an OH radical to yield a carbonyl group, and these reactions are also filtered.[14,15] Additionally, intramolecular hydrogen shifts that move an H atom from a hydroperoxide group to a carbon-centered radical (i.e., QOOH → RO_2) are removed. For RO radicals, there are three canonical reaction pathways that are filtered out:[69] H-atom abstraction by O_2 to yield HO_2 and a carbonyl group, fragmentation to yield an alkyl radical and carbonyl, and intramolecular H-atom transfer (RO → QOH). For RO_2 radicals, the dissociation of the RO_2 radical to R + O_2 and the recently reported RO_2 → QOOH intramolecular H-atom transfer that represents the key step in atmospheric autoxidation are filtered out. While the intramolecular H-atom transfer of RO_2 radicals is not currently a part of standard oxidation schemes, this mechanism has at this point been reasonably well-studied and is now commonly included in

https://doi.org/10.1021/acs.jpca.1c04297
J. Phys. Chem. A 2021, 125, 6772−6788

treatments of atmospheric oxidation chemistry. Therefore, this once-uncanonical reaction type now ought to be incorporated into our canonical understanding of atmospheric oxidation chemistry. Following filtering, the remaining reactions which are both fast and uncanonical are manually categorized based on their reactants and products.

3. RESULTS AND DISCUSSION

The full reaction dataset contains 2×10^6 total reactions, 4882 of which are unique, fast reactions of R, RO, and RO_2 radicals. These include unimolecular reactions and reactions with molecular oxygen. Reactions between organic radicals are not included in this dataset as they are not usually fast enough to compete at typical atmospheric radical concentrations and are not the focus of this work (see Figure S1 and the accompanying Supporting Information text). Of the 4882 unique, fast reactions, 1094 reactions are found to be uncanonical. Overall, the number of unique reactions found is indicative of the diverse chemistry available to organic radicals in the atmosphere.

In this section, we begin by demonstrating the utility of RMG as a reaction discovery tool, by exploring how recently reported chemistry is represented in the RMG-generated dataset. We show that our approach captures the recently reported RO_2 H-shift isomerization, the critical step in atmospheric autoxidation, and even qualitatively captures the SAR associated with this mechanism. Next, we categorize the filtered uncanonical reaction dataset into 12 reaction categories, as shown in Figure 3. These categories include recently reported uncanonical reaction mechanisms, including a hydroperoxy alkyl radical (QOOH) ring-closure reaction to yield a cyclic ether and an OH radical, analogous to the IEPOX formation pathway in the oxidation of isoprene (reaction 1 in Figure 3), and the ring-closure reactions of unsaturated radicals to yield cyclic alkyl radicals (reactions 2−4 in Figure 3), which have also been previously reported for a variety of unsaturated systems.

We then present several examples of novel categories of radical reactions that appear in the dataset, most importantly a radical−carbonyl cyclization mechanism, which has been previously unreported in the atmospheric literature but may be an important step in the atmospheric oxidation of carbonyl species.

3.1. RO_2 Radical H-Atom Shifts in the RMG Dataset—A Test Case for the Reaction Discovery Approach. RO_2 H-atomshifts are an example of a recently reported reaction channel that has since been found to be so ubiquitous that it now ought to be considered part of the canonical atmospheric oxidation chemistry. We therefore begin by demonstrating that the method presented in this work can give insights into the importance of RO_2 shifts at atmospheric temperatures. The fast RMG reaction dataset contains 1504 unique RO_2 H-shift reactions; the majority of these are 1,4, 1,5, and 1,6 H-atom shifts. We also find a small number of 1,3 and 1,7 H-atom shifts. 1,3 shifts are likely to be slow, and the majority of these shifts do not make it past the fast filtering step. 1,7 H-atom shift rates, on the other hand, are often of the same magnitude as that of 1,5 and 1,6 H-atom shift rates.[70] Their absence in the fast dataset is likely a consequence of the choice of pentane as a model system—only a small number of RO_2 reactant radicals that can undergo a 1,7 shift are likely to be encountered in the mechanism generation process, and hence, the 1,7 shifts are underrepresented in this particular dataset.

This result suggests that RO_2 isomerization reactions may be atmospherically important; however, the fast filtering step leaves substantial room for uncertainty in rate constants, with reactions with rate constants near the low cutoff less likely to be important. The distribution of rates associated with these reactions is presented in Figure 4. Because atmospheric RO_2

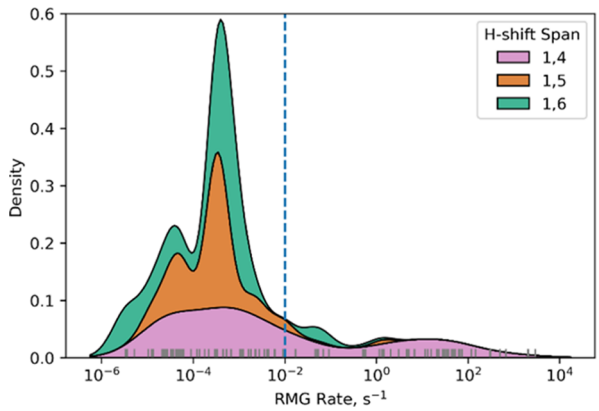

Figure 4. Gaussian kernel density estimate for the distribution of RO_2 H-atom shift reaction rate constants encountered in the filtered RMG dataset. The distribution is colored according to the span of the intramolecular H-atom shift. Note that a small number of 1,3 and 1,7 shifts are included in the filtered dataset, but the areas associated with their distributions are too small to be seen. Short gray lines on the bottom axis represent individual rate constant predictions. RO_2 H-atom shifts with rates above 0.01 s^{-1} (dashed line) are fast enough to compete with traditional RO_2 removal processes under atmospheric conditions.[20]

lifetimes rarely exceed 100 s, unimolecular RO_2 reactions must have rates that exceed 0.01 s^{-1} in order to outcompete more traditional removal processes in the atmosphere in pristine conditions.[20] While the majority of the RO_2 isomerization rate constants found in the RMG dataset are below this value, there is a sizable tail, representing about 15% of the RO_2 isomerization reactions, that are above 0.01 s^{-1}. If this threshold is extended to 0.001 s^{-1} (fast enough to account for ca. 10% of the removal of a given RO_2 radical relative to traditional bimolecular pathways), the portion of RO_2 H-shift rate constants that exceed this value rises to about 27%. This result is consistent with what is now known to be true about RO_2 isomerization reactions: while most are too slow to be of atmospheric significance, many are fast enough to compete with more traditional RO_2 removal pathways.

Next, we assess whether the presence of fast RO_2 H-atom shifts in the RMG dataset is merely coincidental, or if this approach accurately captures which H-atom shifts are likely to be fast. In Figure 5, we compare the rates predicted by RMG to those predicted by a recently published SAR for RO_2 H-atom shifts.[39] Here, we exclude RO_2 radicals with three or more functional groups (which can be formed late in the reaction networks) to avoid the uncertainties in the SAR associated with multifunctional species. The H-atom shifts are sorted based on the identity of the α substituent (i.e., the substituent on the same carbon as the migrating H-atom), as shown in Figure 5. The y-axis shows the ratio of the rate for the H-atom shift reaction in RMG to that from the SAR, with a value of 1 indicating agreement between the RMG rate prediction and that from the SAR. The colors of each point are based on the absolute rate predicted by the SAR (given in Figure S2).

https://doi.org/10.1021/acs.jpca.1c04297
J. Phys. Chem. A 2021, 125, 6772−6788

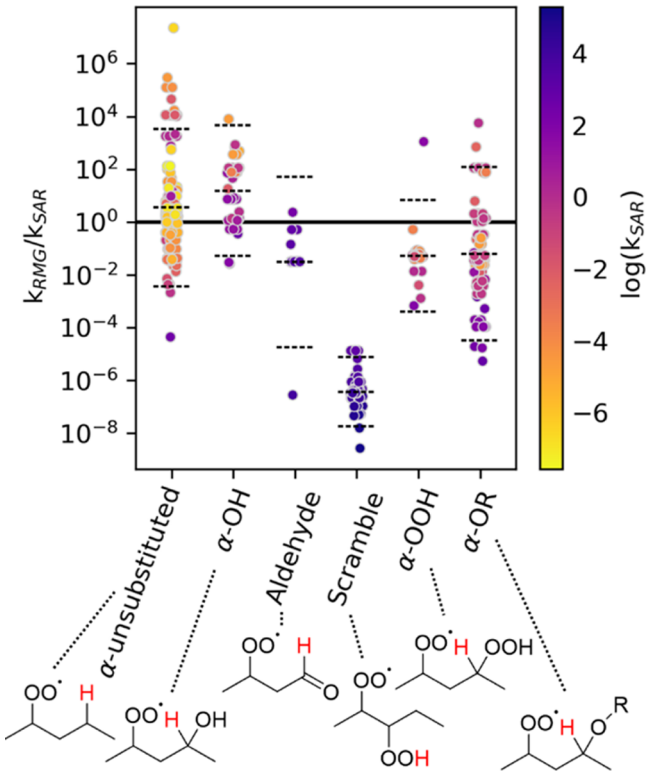

Figure 5. Ratio of the RMG-predicted rate constant (k_{RMG}) to the SAR-predicted rate constant (k_{SAR})[39] for all of the H-atom shift reactions of mono- and bifunctionally substituted RO_2 radicals in the filtered RMG dataset, plotted on a logarithmic scale. Each point represents an individual unique H-atom shift reaction. The points are sorted according to the substituent on the carbon that bears the hydrogen that is shifted in the reaction. The chemical structure for an example reactant RO_2 radical for each category is shown below the graph; the red H atom is the one undergoing the intramolecular hydrogen transfer reaction. Other structures are possible, including additional substituents on other carbons and different H-atom shift spans. The coloring of each point represents the value of k_{SAR}, again on a logarithmic scale. A point falling at a k_{RMG}/k_{SAR} of 1 (solid black line) represents a reaction for which the RMG and SAR predictions are equal. Within each category of the H-atom shift, we show the mean of k_{RMG}/k_{SAR} (central dashed black line) and a 95% confidence interval associated with this ratio (outer dashed black lines), assuming a normal distribution. Summary statistics associated with these data are presented in Table 1.

Descriptive statistics associated with the data presented in Figure 5 are given in Table 1. With the exception of the hydroperoxide "scrambling" reaction, which is discussed below, the results show that on average, the types of H-atom shifts encountered in the dataset are reasonably well represented by RMG.

Table 1. Summary Statistics Associated with H-Atom Shift Reactions Presented in Figure 5

H-shift category	mean($\log(k_{RMG}/k_{SAR})$)	$\sigma(\log(k_{RMG}/k_{SAR}))$	N
aliphatic	0.5	1.6	210
α-OH	1.2	1.3	39
scramble	−6.4	0.7	57
aldehyde	−1.5	1.6	13
α-OOH	−1.3	1.1	25
α-OR	−1.2	1.7	106

The "scrambling" reaction, the shift of a hydrogen atom from the hydroperoxide substituent of an RO_2 radical to the oxygen-centered radical site, yielding a new RO_2 radical rather than QOOH, is systematically underestimated in RMG (by ∼6 orders of magnitude). The SAR for the scrambling process is uncertain as it involves a scaling procedure that is poorly constrained, but it is unlikely that it overestimates the scrambling rate by anywhere near this amount.[39] The underestimation of the scrambling reaction rate points to insufficient parameterization of this reaction in RMG. More generally, this result shows that certain reactions can be so uncertain in RMG that they may be missed by the fast filtering step, representing a potential weakness in this approach. However, this appears to be the case for only one class of RO_2 H-atom shifts out of many, suggesting that severe errors such as this are relatively rare.

For all other categories in Figure 5, the RMG-predicted rates on average capture the same behavior as the SAR does. However, there is considerable variability in the fidelity to the SAR for individual reaction rates within each category. For the α-unsubstituted H-shift category, which includes the largest number of fast reactions, RMG-predicted rates range from ∼4 orders of magnitude lower than the SAR rate to ∼7 orders of magnitude higher. As shown in Figure S3, some of this variability can be attributed to the effects of additional substituents on the rates. For example, while the SAR predicts that a carbonyl group in the β position endo to the transition-state ring increases the H-atom shift rate, RMG appears to systematically overestimate this effect as compared to the SAR. There are also some limitations to the accuracy of the SAR itself—recent work has shown that, particularly for multifunctional species, *ab initio* calculations for individual rate constants can differ from SAR predictions by as much as a factor of 40.[71] Nevertheless, the dataset taken as a whole gives a picture of the kinds of RO_2 H-atom transfer reactions that are likely to be of atmospheric importance, one which is consistent with what the SAR predicts.

While not quantitatively accurate for individual reactions or networks, the dataset gives valuable insights into RO_2 radical H-atom shifts and their potential atmospheric importance. Because the autoxidation mechanism is a well-studied phenomenon in combustion chemistry, the H-atom shifts involved are generally well-parameterized in RMG. Extending the rate information to lower temperatures is not trivial and is made even more difficult by the potential involvement of quantum mechanical tunneling effects for H-atom transfer reactions in particular. Despite the uncertainties involved, the RO_2 H-atom shift example provides a proof of concept for this screening approach.

3.2. Uncanonical Radical Chemistry in the RMG Dataset. We next turn our attention to the uncanonical reaction dataset. We find 12 categories of reactions, as shown in Figure 3. This set of reactions includes several recently reported reaction mechanisms that have since been suggested to be of atmospheric significance: cyclic ether formation from QOOH radicals and unsaturated radical cyclization and ring-opening reactions (reactions 1−3 in Figure 3). We begin by demonstrating that our approach captures these recently described reactions as well, lending further confidence to its ability to discover uncanonical mechanisms. We then turn our attention to the previously unreported mechanisms found in the RMG dataset, shown as reactions 4−12 in Figure 3. Summary statistics associated with each reaction type are

https://doi.org/10.1021/acs.jpca.1c04297
J. Phys. Chem. A 2021, 125, 6772−6788

Table 2. Summary Statistics Associated with Each "Uncanonical" Reaction Category Presented in Figure 3

	reaction category	product description (subcategories)		N	geometric mean (k) s^{-1}	geometric standard deviation (k)	arithmetic mean (k/k_{total}), s^{-1}	arithmetic $\sigma(k/k_{total})$
1	cyclic ether formation	three-membered ring		193	1.8×10^4	1.5	7.0×10^{-4}	9.3×10^{-4}
		six-membered ring		53	3.4×10^7	16	0.76	0.20
2	RO_2-alkene cyclization	three-membered ring	endo	0				
			exo	3	4.9×10^2	49	0.98	2.7×10^{-2}
		four-membered ring	endo	0				
			exo	3	4.5×10^{-1}	1.3	1.9×10^{-2}	3.1×10^{-2}
		five-membered ring	endo	14	9.4×10^{-1}	2.2	0.18	0.30
			exo	27	3.2×10^5	6.4	0.87	0.24
		six-membered ring	endo	27	1.3×10^4	2.2	0.13	0.24
			exo	15	7.2×10^3	60	0.84	0.35
		seven-membered ring	endo	8	7.9×10^2	9.6	0.42	0.49
			exo	0				
3	RO−alkene cyclization			4	6.5×10^4	4.9	0.32	0.44
4	R−alkene cyclization			14	5.3×10^4	3.1	4.4×10^{-3}	6.2×10^{-3}
5	cyclic R ring opening	RO_2		68	2.9×10^8	1.4×10^2	0.65	0.40
		RO		32	1.5×10^{12}	29	0.82	0.33
		R		18	3.7×10^8	1.3×10^4	0.19	0.34
6	RO_2−carbonyl cyclization	five-membered ring RO		53	1.3×10^1	75	0.81	0.31
		six-membered ring RO		41	4.2×10^1	1.1×10^2	0.65	0.40
		seven-membered ring RO		7	1.3×10^{-5}	1	3.7×10^{-4}	1.1×10^{-4}
7	R−carbonyl cyclization	five-membered ring RO		13	1.5×10^4	1	0.71	0.43
		six-membered ring RO		2	4.4×10^3	1	0.61	0.54
8	R−carbonyl cyclization	five-membered ring RO		11	2.7×10^4	12	2.0×10^{-2}	6.5×10^{-2}
		six-membered ring RO		4	4.1×10^3	1	3.3×10^{-4}	4.0×10^{-6}
		five-membered ring R		10	2.1×10^3	1.8	1.4×10^{-4}	1.0×10^{-5}
		six-membered ring R		13	1.0×10^4	1.4	4.8×10^{-4}	2.3×10^{-4}
		seven-membered ring R		1	3.5×10^4		1.2×10^{-3}	
9	oxy(di)oxane ring opening	RO_2		70	1.9×10^{11}	13	0.35	0.37
		peroxy ester R radical		79	6.2×10^{10}	70	0.27	0.34
		RO		4	6.9×10^{10}	19	0.27	0.49
		ester R radical		18	4.7×10^{12}	6.5×10^4	0.87	0.32
10	RO_2−hydroperoxide ozonide formation			183	1.5×10^{-4}	21	7.9×10^{-3}	3.2×10^{-2}
11	RO−hydroperoxide endocyclic peroxide formation			5	3.6×10^{-1}	1.8×10^3	7.9×10^{-3}	1.2×10^{-2}
12	RO H-atom shift to vinoxy (keto−enol tautomerization)			10	3.7×10^8	21	0.69	0.40

shown in Table 2. Several of these reactions are shown to be potentially important atmospheric pathways and are identified as promising targets for further studies via experiments or more detailed calculations.

3.2.1. Cyclic Ether Formation. Reaction 1 in Figure 3 involves the ring closure of a hydroperoxy-substituted R radical, which yields a cyclic ether species and an OH radical coproduct. The key ring-closing step in the IEPOX formation pathway discussed in Section 1 is one example of this reaction. The ring closure is mainly in competition with O_2 addition to yield a new, hydroperoxy-substituted RO_2 radical. As with RO_2 H-atom shifts, cyclic ether formation reactions of hydroperoxy-substituted R radicals have been known for some time in low-temperature combustion chemistry,[72−77] but their detailed, structure-dependent kinetics are not as well-constrained, particularly at atmospherically relevant temperatures.[50]

Epoxide (three-membered cyclic ether) formation is the most well-parameterized cyclic ether formation reaction, with a typical thermal unimolecular rate coefficient of around 10^3 to 10^4 s^{-1} at 298 K.[45,50] This is too slow to compete with the addition of molecular oxygen under thermal conditions, which occurs with a typical pseudo-first-order rate constant k'_{O_2} ($k_{R+O_2}[O_2]$) on the order of 10^7 to 10^8 s^{-1};[78,79] epoxide formation usually can only compete when the β-hydroperoxy alkyl radical reactant is chemically activated. However, recent theoretical work has shown that substituent effects can substantially enhance the thermal rate of the epoxide formation reaction, allowing for epoxide formation under thermal conditions for some species as well.[50]

In the filtered RMG dataset, we find 246 unique cyclic ether formation reactions, 193 of which form epoxides and 53 of which form six-membered oxanes. Four- and five-membered ring-closing reactions are predicted as well but do not make it past the fast filtering step. This indicates that these reactions have thermal rates that are too slow to compete with the O_2 addition pathway under atmospheric conditions. The distribution of RMG-predicted rates associated with these reactions is

https://doi.org/10.1021/acs.jpca.1c04297
J. Phys. Chem. A 2021, 125, 6772−6788

shown in Figure S4. The rates for epoxide formation fall between 10^4 and 10^5 s^{-1}, in reasonably good agreement with the reported thermal rate of IEPOX formation of 10^3 to 10^4 s^{-1}.[45] The results do not capture the substituent effect described above, and thus, the thermal rates predicted for cyclic ether formation are much slower than k'_{O_2}. Nevertheless, the cyclic ether formation reactions make it through the "fast" filtering step and hence are identified as a potentially important reaction pathway. This example illustrates why using a low cutoff factor ($k/k_{total} = 10^{-4}$) is necessary when filtering for "fast" reactions. As discussed in Section 2, the approach used herein does not account for chemical activation. However, using the low cutoff factor allows processes that may only be competitive due to chemical activation to make it past the "fast" filtering step and receive further consideration.

We also find oxane formation reactions in the RMG dataset, involving the ring closure of a δ-hydroperoxyalkyl radical. The RMG-predicted rates for oxane formation fall between 10^7 and 10^8 s^{-1}. This is in conflict with the recently published *ab initio* results that suggest that oxane formation (similar to the formation of four- and five- membered ring formation) is substantially slower than the analogous epoxide formation reaction under thermal conditions, both for substituted and unsubstituted systems, due to the entropic cost associated with the loss of conformational freedom from the ring closure.[50] Though larger cyclic ether formation reactions are possible at the elevated temperatures encountered in combustion,[74,80,81] *ab initio* calculations suggest they are unlikely to be important under atmospheric conditions. Oxane formation therefore appears to be systematically overestimated in RMG. This is an example of a case where the RMG results suggest further investigation of a reaction pathway, but more detailed quantum calculations reveal that the pathway is unlikely to compete with the more traditional removal mechanisms, at least under thermal conditions. Cases like this are to be expected due to the uncertainty associated with RMG results and highlight the need for further quantum mechanical or experimental investigation of any new mechanisms suggested by RMG calculations.

3.2.2. Unsaturated Radical Cyclization Reactions. Reactions 2−4 in Figure 3 involve intramolecular cyclization reactions of unsaturated RO_2, R, and RO radicals. Here, the radical center attacks a C−C double bond, yielding a new, cyclic R radical. Figure 6 shows the predicted rates for these reactions. Figure 6a shows the absolute rates associated with each of these reaction categories, while Figure 6b shows the ratios of the rates of the reaction of interest to the total reaction rates of the reactant radicals (k/k_{total}). The calculation of k_{total} is described in Section 2.2. Summary statistics associated with the data presented in Figure 6 are given in Table 2.

For the RO_2 ring closure (reaction 2 in Figure 3), the terminal oxygen of the RO_2 radical attacks one of the double bonded carbons, leading to a cyclic R radical with an endocylic peroxide (C−O−O−C). The oxygen can be added either to the proximal end of the double bond, yielding a radical site external to the ring (exocyclic), or to the distal end, yielding a radical site on one of the ring carbons (endocyclic). This mechanism is known to be important in the oxidation of aromatic species[82−84] and has been shown via quantum mechanical calculations to compete with H-shift reactions for unsaturated peroxy radicals.[85−88] It represents an extension of

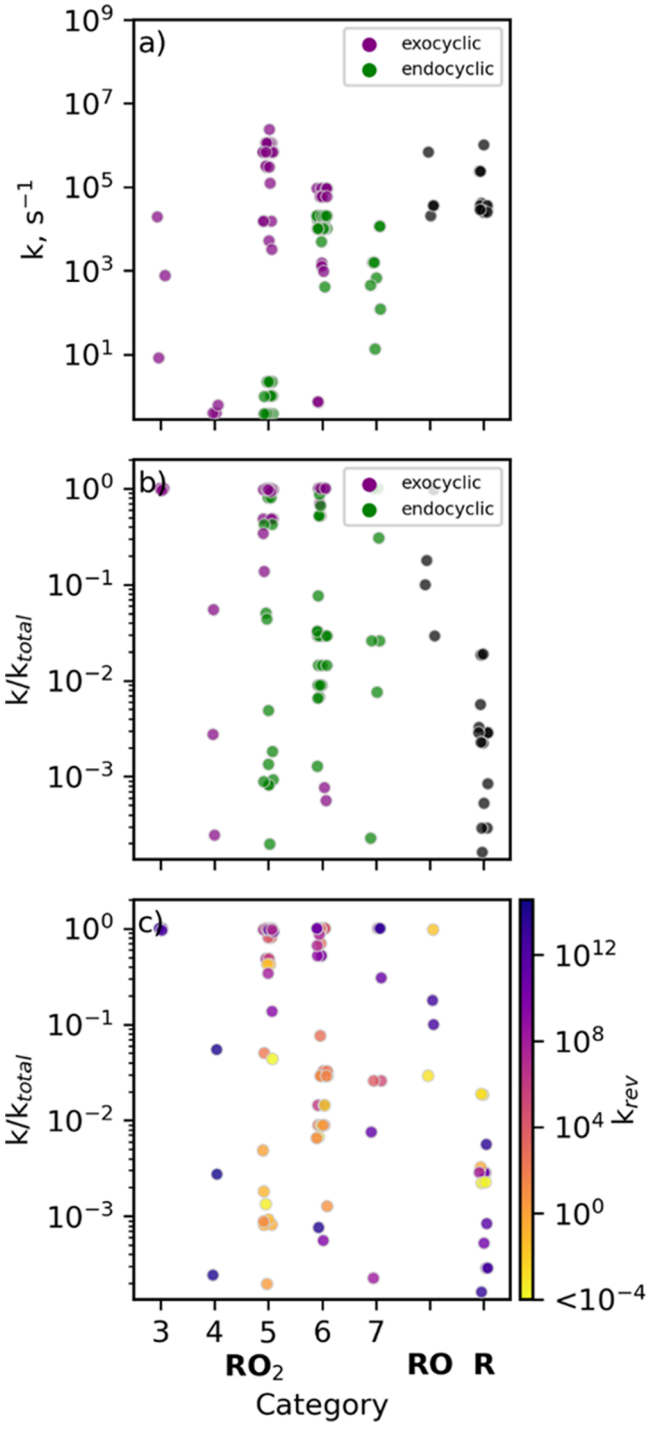

Figure 6. (a) Rate constants for unsaturated radical ring-closing reactions (reactions 2−4 in Figure 3) from the filtered RMG dataset, sorted according to the identity of the reactant radical (RO_2, RO, and R). For the RO_2 radical, the results are further categorized by the ring size of the product R radical and identified based on whether the product radical is endocyclic or exocyclic. (b) Ratio of the rate constant of the unsaturated radical ring-closure reaction to the total removal rate for the reactant radical (k/k_{total}). (c) Same as in (b), but with points colored according to the rate of the reverse (ring-opening) reaction. The reverse reaction is in competition with O_2 addition to the product radical, with a typical rate constant on the order of 10^7 to 10^8 s^{-1}.[78,79]

https://doi.org/10.1021/acs.jpca.1c04297
J. Phys. Chem. A 2021, 125, 6772−6788

the atmospheric autoxidation scheme discussed above. However, to date, there exist only sparse studies on this cyclization mechanism for individual species.

In Figure 6a, we show the RMG-generated rates for the RO_2−alkene ring-closure reactions found in the dataset. We find 97 unique RO_2−alkene cyclization reactions, spanning ring sizes containing three−seven atoms. Most of these (83 out of 97) involve the formation of five- and six-membered rings. For the five-membered ring formation, the rates for exocyclic radical formation are on the order of 10^3 to 10^7 s^{-1}, while those for endocyclic radical formation are significantly slower on the order of 10^0 to 10^1 s^{-1}. The difference between exocyclic and endocyclic radical formation reactions for six-membered rings is less pronounced, with most of the rates falling between 10^3 and 10^6 s^{-1}, though on average the formation of exocyclic radical is slightly faster.

For the remaining ring sizes (three-, four-, and seven-membered rings), only a few reactions are found for each. In general, when reactions show up only rarely in the filtered dataset, there are two possible explanations: either the reactant radical that allows for such a reaction is rarely encountered in the network generation process or the reactant radical is available, but the reaction rates are too slow to make it past the "fast" filtering step. Both explanations play a role here, as discussed in the Supporting Information.

There are two key factors that determine the potential importance of the unsaturated RO_2 ring-closure reaction is likely to be in the atmosphere. The first is the ratio of the ring-closure reaction rate to the total removal rate (k/k_{total}) for the RO_2 radical reactant, plotted in Figure 6b. For the five- and six-membered ring formation reactions, we find average k/k_{total} values of 0.6 and 0.4, respectively, suggesting a substantial loss of these RO_2 radicals via this cyclization pathway, at least under the low NO/HO_2 conditions considered here. In some cases, the RMG-predicted rates are sufficiently fast that the ring closure could compete with bimolecular processes even under more polluted conditions.

Second, unlike the epoxide formation reaction, which yields two fragmentation products, the RO_2−alkene cyclization reaction is reversible. Therefore, its importance is governed not only by the rate at which the cyclization product forms but also by the rate of the reverse ring-opening reaction (with the rate constant k_{rev}) relative to other loss processes of the cyclization product. In fact, such fast R radical ring-opening reactions appear as an additional uncanonical reaction type in the filtered dataset (reaction 5 in Figure 3). The main removal process in competition with the ring opening for the product cyclic R radical is the O_2 addition reaction, with a pseudo-first-order rate constant (k'_{O_2}) on the order of 10^7 to 10^8 s^{-1}.[78,79] In Figure 6c, each point is colored according to the k_{rev} rate constant. For the five- and six-membered ring-closing reactions, the mean k_{rev} is on the order of 10^9 s^{-1}, slightly larger than the typical k'_{O_2} but slow enough that in many cases the two processes will be competitive. For a number of the cyclization reactions with the highest k/k_{total} ratios, k_{rev} is on the same order as or lower than k'_{O_2}, suggesting that some of these reactions may be of atmospheric significance.

Here, we have explored only the effects of the ring size and exocyclic versus endocyclic radical formation on the rate constants. Given the variation within a single ring size and product radical type, it is likely there are additional substituent effects (e.g., from oxygen-containing functional groups) on the ring-closure rates, which are not investigated in detail here. Nevertheless, the results highlight these unsaturated radical ring-closure reactions as important targets for systematic exploration.

Reactions 3 and 4 in Figure 3 are cyclization reactions of unsaturated RO and R radicals. These reactions are analogous to the RO_2−alkene ring-closure reaction described above. However, in contrast to the RO_2−alkene ring-closure reaction, which primarily competes with bimolecular reactions with NO and HO_2, the R and RO ring-closure reactions compete with much faster processes.

The ring-closure reaction for unsaturated RO radicals (reaction 3 in Figure 3) has been proposed previously for RO radicals encountered in the oxidation of isoprene and monoterpenes[89] and has been suggested as a possible explanation for anomalously low yields of expected oxidation products from β-pinene[40] but has not been explored systematically in the literature. This reaction competes with several possible typical RO radical reactions (H-atom transfer, fragmentation, and reaction with O_2), whose relative importance depends on the structure of the RO radical. This reaction type appears only four times in the filtered RMG dataset, likely due to the limited way RO radicals are included in the dataset (see Section 2.2). The ring-closure reaction has a mean rate constant on the order of 10^4 s^{-1} and a relatively high average k/k_{total} of 0.3. As with the RO_2−alkene cyclization, the importance of the ring-closure reaction in the atmosphere also depends on the relative values of the reverse ring-opening rate constant (k_{rev}), which varies substantially among the few examples encountered here. From the limited number of these reactions encountered in this dataset, it is difficult to make conclusions about this chemistry, and further investigation is needed to understand the effects of the ring size, exo- versus endocyclic radical formation, and other substituents. Nevertheless, the RMG results suggest, in agreement with the few previous discussions of these reactions, that RO−alkene ring-closure reactions are a promising target for further study.

We find only 14 R−alkene ring-closure reactions (reaction 4 in Figure 3) in the filtered RMG dataset. Here, the ring-closure reaction is in competition with oxygen addition, where the pseudo-first-order rate constant k_{O_2} is on the order of 10^7 to 10^8 s^{-1}. Hence, even though the R−alkene ring-closure reaction is predicted to have an average rate constant on the order of 10^5 s^{-1}, it is unlikely to be important under thermal conditions. As with the epoxide formation reaction, however, we cannot rule out the possibility of its importance due to chemical activation, particularly in cases where the parent R radical is formed by OH addition rather than H-atom abstraction.

3.2.3. Carbonyl Radical Cyclization Reactions. While the unsaturated radical cyclization reactions described in the previous section have received some limited attention as possible atmospheric reaction mechanisms, the analogous, isoelectronic reactions for carbonyl-containing radicals have been largely overlooked. In the RMG dataset, we find a number of carbonyl radical cyclization reactions. These are primarily RO_2−carbonyl cyclizations (reaction 6 in Figure 3), but we also find several involving RO and R radicals (reactions 7 and 8 in Figure 3, respectively). In most cases (131 out of 155), the radical attacks the carbon of the carbonyl group, resulting in a cyclic alkoxy radical which can then undergo

https://doi.org/10.1021/acs.jpca.1c04297
J. Phys. Chem. A 2021, 125, 6772−6788

subsequent ring-opening reactions (reaction 9 in Figure 3). In the remaining 24 cases, an R radical attacks the oxygen of the carbonyl group, yielding a cyclic R radical with an endocyclic O atom; this pathway is not observed for RO and RO_2 radicals. Figure 7 shows the rate and k/k_{total} distributions associated with these carbonyl ring-closures.

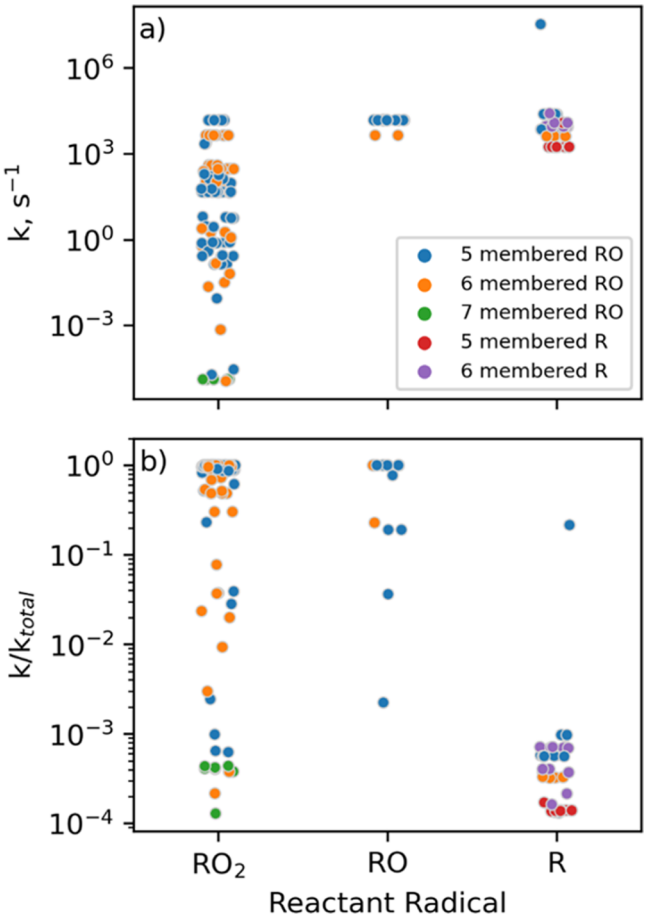

Figure 7. (a) Rate constants for carbonyl−radical ring-closing reactions (reactions 6−8 in Figure 3) from the filtered RMG dataset. Points are sorted along the *x*-axis according to the identity of the reactant radical (RO_2, RO, and R). Points are colored according to the identity of the product of the cyclization reaction (five-, six-, and seven-membered RO and R radicals) as shown in the figure legend. (b) Ratio of the rate constant of the unsaturated radical ring-closure reaction to the total removal rate for the reactant radical (k/k_{total}).

101 unique RO_2−carbonyl cyclization reactions are found in the filtered RMG dataset, with rate constants spanning a range from 10^{-4} to 10^{4} s^{-1}. As shown in Figure 7a, the fastest of these rates are associated with the formation of five- and six-membered rings, while the formation of seven-membered rings is significantly slower. For five- and six-membered ring formations, this process is often one of the fastest reaction pathways available, with mean k/k_{total} values of 0.8 and 0.7, respectively (Figure 7b). The seven-membered ring formation has an average k/k_{total} of 0.0004, suggesting this is a minor pathway (although this may be the result of the limited inclusion of species that can form seven-membered rings in the dataset). Hence, from here on, we restrict our discussion to five- and six-membered ring formations. To our knowledge, the RO_2−carbonyl ring-closure reaction has not been observed experimentally. It has been discussed only once before, in a recent theoretical study by Sebbar et al., which shows that the 2-butanone-4-peroxy radical can cyclize to form a five-membered oxydioxolane radical product.[90] They show that this cyclization proceeds via a submerged barrier (relative to the R + O_2 addition that forms the RO_2 radical) and hence conclude that this pathway may be important in atmospheric and combustion systems.[90]

As with other RO_2 unimolecular reactions, the k/k_{total} of these ring-closure reactions depends on the concentrations of NO and HO_2. Because they are predicted to be so fast, with rate constants on the order of 10^{4} s^{-1}, these carbonyl ring-closure reactions would have high k/k_{total} values even at higher NO and HO_2 concentrations, suggesting that this chemistry may dominate the chemistry of some carbonyl-substituted RO_2 radical reactivity even in polluted environments.

Reactions 7 and 8 in Figure 3 are carbonyl ring-closure reactions for RO and R radicals, with rate constants shown in Figure 7. Each of these reaction types is far less common in the RMG dataset, with only 39 R−carbonyl cyclization reactions and 15 RO−carbonyl cyclization reactions. The RO−carbonyl cyclization reactions (reaction 7 in Figure 3) have a mean rate constant on the order of 10^{4} s^{-1}. This is on the same order or faster than many of the competing RO reactions, and we find an average k/k_{total} for this category of 0.7, indicating that such a cyclization reaction could be an important pathway. The low number of these reactions encountered is again due to the low number of alkoxy radicals included in the dataset and precludes gaining a more detailed understanding of this chemistry from the RMG dataset alone. Nevertheless, this work indicates that these RO−carbonyl cyclization reactions are a promising target for further study. For the R−carbonyl cyclization reaction (reaction 8 in Figure 3), in which the radical center can attack either the C or the O of the carbonyl group, the mean rate is on the order of 10^{4} s^{-1}, substantially lower than that of the competing O_2 addition pathway. This reaction is therefore unlikely to be important under thermal conditions, though we cannot rule out its enhancement by chemical activation.

Both the RO_2−carbonyl cyclization reaction and the RO−carbonyl cyclization produce a new RO radical. The newly formed cyclic RO radical may have quite different chemistry than a typical, linear RO (Figure 1). Because the ring structure reduces conformational flexibility, the intramolecular H-atom shift is generally unavailable and does not appear in the RMG dataset for the cyclic RO radicals. RMG predicts pseudo-first-order rates for the H-atom abstraction reaction on the order of 10^{5} s^{-1}, in agreement with literature values for the reaction of O_2 and secondary RO radicals.[91] This is substantially slower than the possible ring opening reactions (reaction 9 in Figure 3), involving the breakage of the new C−O bond (the reverse of the ring-closing reaction) or of the adjacent C−C bond (forming a new R radical with a peroxy ester or ester moiety). Note that this C−C bond-breaking reaction is equivalent to a typical, RO radical β-scission fragmentation reaction. However, because the radical here is cyclic, the bond breaking results in a single, functionalized (peroxyester) R radical rather than two fragments.

As with the unsaturated radical cyclization reactions discussed above, if the rate of the C−O bond-breaking reaction greatly exceeds the rate of the C−C bond-breaking reaction, it will limit the importance of the overall cyclization process. However, unlike in the unsaturated radical ring-closure reactions described above, in which the competing O_2

https://doi.org/10.1021/acs.jpca.1c04297
J. Phys. Chem. A 2021, 125, 6772−6788

addition rate is largely independent of the molecule in question, the C−C bond-breaking rate is likely to be highly structure-dependent. Figure 8 shows the rate constants

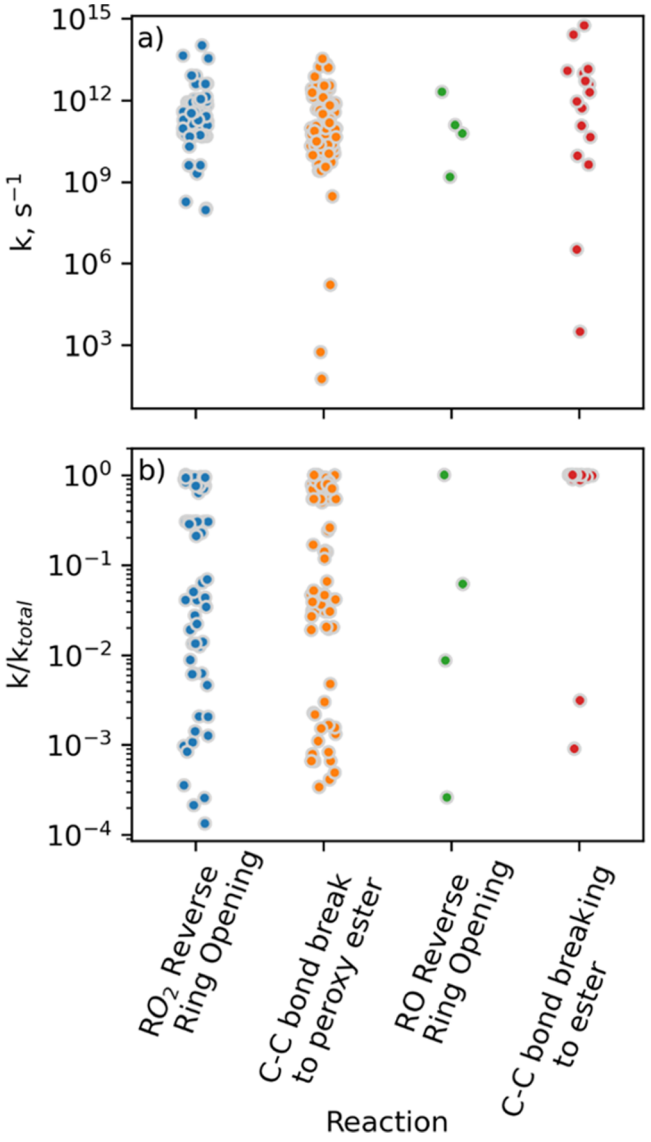

Figure 8. (a) Rate constants for cyclic RO radical ring-opening reactions (reaction 9 in Figure 3) from the filtered RMG dataset, sorted according to the identity of the reactant radical (RO_2, RO, and R). (b) Ratio of the RO ring-opening reaction to the total removal rate for the reactant radical (k/k_{total}).

associated with cyclic RO radical ring-opening reactions. Two outliers have been removed from this plot as they are found to be predicted as the result of an error (which has since been addressed) in the version of RMG used in this work; see the Supporting Information for additional information. The rates for the C−C bond-breaking reactions and C−O bond-breaking (reverse ring-opening) reactions are of similar magnitudes, which overall suggests that for both the RO and RO_2 carbonyl cyclization reactions, the two possible removal pathways for the cyclic RO product will compete with one another. Sebbar et al. found that the cyclic alkoxy radical formed from the cyclization of the 2-butanone-4-peroxy radical undergoes the C−C bond-breaking reaction.[90] Different processes are likely to dominate for different cyclic RO radicals. A more complete understanding of this competition is needed and would require both detailed master equation modeling simulations of the chemistry on the multiple-well potential energy surface associated with these reactions and systematic investigation of substituent effects.

The fate of the R radical formed from the C−C bond-breaking reaction is also important in assessing the atmospheric impact of this new reaction pathway. Sebbar et al. suggest that for the model system they investigated, the next step is an O−O bond breakage, which would lead to two fragmentation products.[90] This bond-breaking reaction is presumably in competition with O_2 addition, which would yield a new, highly functionalized RO_2 radical.

Overall, the present results from RMG, together with the quantum mechanical results presented by Sebbar et al., suggest that the RO_2−carbonyl ring-closure reaction may be of importance in the atmosphere. Thus, this reaction and the fate of the resulting cyclic RO radical represent promising targets for future experimental and theoretical study.

3.2.4. Other Uncanonical Reactions in the RMG Dataset. The carbonyl cyclization reactions described above represent the most promising target for further study in the RMG dataset. However, we also find several other uncanonical reactions in the filtered dataset. Herein, we briefly discuss the most promising of these reactions (reactions 10−12 in Figure 3) in terms of their potential atmospheric importance and relevance for further study. In addition, 54 of the reactions in this filtered dataset do not belong to any of the categories shown in Figure 3—these remaining reactions are expected to be of limited importance and are presented in the Supporting Information (Figure S5 and the accompanying text).

Reaction 10 in Figure 3 is an RO_2−OOH ring-closure reaction which appears 183 times in the filtered RMG dataset. The rate and k/k_{total} distributions associated with this reaction category are presented in Figure S6. This reaction results in the formation of a six-membered ozonide-like species and an OH coproduct, a process that is isoelectronic with the hydroperoxy-substituted R radical ring closure to oxane (reaction 1 in Figure 3). Because this reaction results in the formation of a closed-shell product, as well as in OH radical production, it is potentially interesting from an atmospheric chemistry perspective. By and large, however, these reactions are predicted to be slow, with a mean rate constant on the order of 10^{-4} s^{-1} and a mean k/k_{total} of 10^{-3}. In this case, chemical activation is unlikely to increase the importance of these reactions because the same β-hydroperoxy substituted RO_2 radicals that can undergo this ring-closure reaction can also undergo a relatively fast H-atom shift, which presumably would also be enhanced by chemical activation and outcompete the ring closure. However, while the mean rate constant for this reaction is quite low, a subset of these reactions (41 out of 183), in which a carbonyl group or an ether is present in the newly formed ring, are significantly faster with rates that exceed 0.01 s^{-1}, suggesting that under limited circumstances, this mechanism could be important.

Analogously, reaction 11 in Figure 3 is an RO−OOH ring-closure reaction (reaction 11 in Figure 3) that appears five times in the dataset; this small number is again due to the limited number of alkoxy radicals encountered. The associated rates are also shown in Figure S6. This reaction results in the formation of a five-membered ring with an endocyclic peroxide and an OH coproduct. These reactions are predicted to be somewhat faster than the corresponding RO_2−OOH reaction

https://doi.org/10.1021/acs.jpca.1c04297
J. Phys. Chem. A 2021, 125, 6772−6788

(reaction 10), with rate constants on the order of 10^{-1} s^{-1}, but compete with much faster reactions than those for RO_2 radicals and thus still have a relatively low mean k/k_{total} of 10^{-3}. The results suggest that this reaction is likely to be at most a minor pathway, though it is difficult to make conclusions from such a small sample.

Reaction 12 in Figure 3 is an untraditional H-atom shift for β-carbonyl-substituted RO, which appears only 10 times in the filtered dataset. The rate and k/k_{total} distributions are presented in Figure S7. This reaction is available only for β-carbonyl-substituted RO radicals, which explains the small number of times it is encountered in the dataset. While RO radicals are known to undergo an intramolecular H-atom shift reaction that yields an OH-substituted R radical, the H-atom shift discussed here is different; the H atom, rather than shifting from the carbon skeleton to the radical center, shifts from the carbon skeleton to the carbonyl oxygen, yielding an enol, analogous to a typical keto−enol tautomerization reaction. This 1,3 H-atom shift might be expected to be quite slow due to the strain associated with the four-membered ring transition state.[92] However, the newly formed C−C double bond provides resonance stabilization of the radical as the reaction converts the reactant RO into a vinoxy radical. This stabilization effect accelerates the reaction; the RMG results predict a reaction rate on the order of 10^{10} s^{-1}, with an average k/k_{total} of 0.7.

As with other unimolecular reactions presented here, we must consider not only the forward rate but also the ratio between the reverse reaction and subsequent reactions of the product radical. In this case, the reverse reaction is quite slow because it would require breaking the resonance stabilization of the newly formed OH-substituted vinoxy radical (the average RMG-predicted reverse reaction rate is on the order of 10^{-15} s^{-1}). However, the forward reaction is quite exothermic (with an average predicted ΔH_{rxn} of −146 kJ mol^{-1}), and it is possible that the reverse reaction is enhanced due to chemical activation. The reverse reaction likely competes with the reaction with O_2, which might add to the vinoxy radical to yield a peroxy radical or abstract an H-atom, yielding a closed-shell dicarbonyl product. Typically, vinoxy radical reactions with O_2 have pseudo-first-order rate constants on the order of 10^5 to 10^6 s^{-1},[64−66] but it is unknown how the alcohol substituent on the vinoxy radical here would affect the O_2 reaction rate. Despite their limited inclusion in this dataset, this reaction category, which represents markedly different chemistry than is typically considered for RO radicals, warrants further study.

4. CONCLUSIONS

Typical approaches to searching for new mechanisms often involve writing out possible transformations by hand and then doing experiments and/or calculations to verify. Given the complexity associated with organic chemistry in the atmosphere, efficient approaches to exploring the full ensemble of available chemical transformations are critical to describing the evolution of atmospheric ROC. The approach described herein represents a far more efficient, inexpensive, and systematic way to carry out initial explorations of the chemical space.

We have used RMG to explore a large portion of chemical space relevant to atmospheric organic chemistry with the goal of screening for uncanonical chemistry of organic radicals. RMG (and other similar programs) are powerful tools for the generation of networks describing the oxidation of individual species or mixtures. The approach presented here, in which RMG is used to scan across a large range of radical species and their possible reactions and estimate their associated kinetics, represents a new application for such tools. We show that this application has the potential to unearth new and potentially important mechanisms in atmospheric organic oxidation.

We encounter several recently appreciated organic radical mechanisms. In particular, we find a substantial number of RO_2 H-atom transfer reactions, the key reaction step in the atmospheric autoxidation pathway. We show that the RMG results qualitatively capture features of the SAR associated with this H-atom transfer mechanism. Further, other recently described uncanonical atmospheric mechanisms (epoxide formation and intramolecular radical addition to alkenes) also appear in the RMG dataset. These "proof of concept" results provide confidence in this approach as a tool in the search for currently overlooked reaction steps in atmospheric oxidation. We then examine several novel reaction types, the most promising of which is a radical−carbonyl ring-closure reaction, which is proposed as a critical target for further study via experiments and more detailed theoretical calculations.

Throughout this work, the potential role of chemical activation in influencing branching ratios or opening new pathways is encountered frequently. In this initial investigation, we assume that all reactions occur under thermal conditions and provide a very low rate cutoff (k/k_{total} = 10^{-4}) in the filtering process. In an approximate sense, this low cutoff allows for the possibility of chemical activation but does not indicate how important it might be and may not capture all chemically activated processes. As discussed above, RMG does have the capability to include chemical activation effects in the network generation process, though this is anticipated to result in a significant increase in the computational cost. It will also complicate the filtering process as each elementary step must be treated not as a standalone reaction but rather in the context of its surrounding potential energy landscape. Nevertheless, a major goal for future work is to incorporate a treatment of chemical activation into both the network generation and filtering process.

In addition to more detailed exploration of the uncanonical mechanisms presented herein and the improvement of the treatment of chemical activation, future work may focus on improving the accuracy of generated networks by adding additional atmospherically relevant training reactions to the RMG database and on expanding the utility of this approach to more complex atmospheric problems. Such work includes extending similar methods to larger and more complex species with branched, cyclic, and aromatic functionalities, as well as systems that contain non-oxygen heteroatoms (e.g., organonitrogen and organosulfur species), and exploring the chemistry of complex mixtures of organic species. Similar approaches may also be used to investigate condensed-phase or interfacial systems. Such extensions will allow for exploration of new areas in the chemical space and may unearth further unexpected mechanisms.

■ ASSOCIATED CONTENT

Supporting Information

The Supporting Information is available free of charge at https://pubs.acs.org/doi/10.1021/acs.jpca.1c04297.

RMG input and output files, code for the filtering algorithm, and additional information on model inputs; effects of β substituents on the RO_2 H-shift rates

https://doi.org/10.1021/acs.jpca.1c04297
J. Phys. Chem. A 2021, 125, 6772−6788

predicted by RMG; and descriptions of and statistics associated with uncategorized reactions and reactions between organic radicals in the filtered dataset (PDF)

AUTHOR INFORMATION

Corresponding Author

Victoria P. Barber − *Department of Civil and Environmental Engineering, Massachusetts Institute of Technology, Cambridge, Massachusetts 02139, United States;* orcid.org/0000-0003-4543-4657; Email: vbarber@mit.edu

Authors

William H. Green − *Department of Chemical Engineering, Massachusetts Institute of Technology, Cambridge, Massachusetts 02139, United States;* orcid.org/0000-0003-2603-9694

Jesse H. Kroll − *Department of Civil and Environmental Engineering and Department of Chemical Engineering, Massachusetts Institute of Technology, Cambridge, Massachusetts 02139, United States;* orcid.org/0000-0002-6275-521X

Complete contact information is available at: https://pubs.acs.org/10.1021/acs.jpca.1c04297

Notes

The authors declare no competing financial interest.

ACKNOWLEDGMENTS

This work was supported by NSF grant CHE-1709993. The authors thank Dr. Mark Goldman and Xiaorui Dong for helpful discussions.

REFERENCES

(1) Guenther, A.; Hewitt, C. N.; Erickson, D.; Fall, R.; Geron, C.; Graedel, T.; Harley, P.; Klinger, L.; Lerdau, M.; McKay, W. A.; et al. A Global Model of Natural Volatile Organic Compound Emissions. *J. Geophys. Res. Atmos.* **1995**, *100*, 8873−8892.

(2) Friedrich, R.; Obermeier, A. Anthropogenic Emissions of Volatile Organic Compounds. In *Reactive Hydrocarbons in the Atmosphere*; Hewitt, C. N., Ed.; Academic Press: San Diego, 1999; pp 1−39.

(3) Klimont, Z.; Kupiainen, K.; Heyes, C.; Purohit, P.; Cofala, J.; Rafaj, P.; Borken-Kleefeld, J.; Schöpp, W. Global Anthropogenic Emissions of Particulate Matter Including Black Carbon. *Atmos. Chem. Phys.* **2017**, *17*, 8681−8723.

(4) Aumont, B.; Camredon, M.; Mouchel-Vallon, C.; La, S.; Ouzebidour, F.; Valorso, R.; Lee-Taylor, J.; Madronich, S. Modeling the Influence of Alkane Molecular Structure on Secondary Organic Aerosol Formation. *Faraday Discuss.* **2013**, *165*, 105−122.

(5) Goldstein, A. H.; Galbally, I. E. Known and Unexplored Organic Constituents in the Earth's Atmosphere. *Environ. Sci. Technol.* **2007**, *41*, 1514−1521.

(6) Atkinson, R.; Arey, J. Atmospheric Degradation of Volatile Organic Compounds. *Chem. Rev.* **2003**, *103*, 4605−4638.

(7) National Resource Council. *Rethinking the Ozone Problem in Urban and Regional Air Pollution*; National Academies Press, 1992.

(8) Fowler, D.; Coyle, M.; Anderson, R.; Ashmore, M. R.; Bower, J. S.; Burgess, R. A.; Cape, J. N.; Cox, R. A.; Derwent, R. G.; Dollard, G. J.; et al. *Ozone in the United Kingdom—Fourth Report of the Photochemical Oxidants Review Group—1997*; The Centre for Ecology and Hydrology, 1997.

(9) Finlayson-Pitts, B. J.; Pitts, J. N. *Chemistry of the Upper and Lower Atmosphere*; Academic Press: San Diego, 2000.

(10) Zhang, Q.; Jimenez, J. L.; Canagaratna, M. R.; Allan, J. D.; Coe, H.; Ulbrich, I.; Alfarra, M. R.; Takami, A.; Middlebrook, A. M.; Sun, Y. L.; et al. Ubiquity and Dominance of Oxygenated Species in Organic Aerosols in Anthropogenically-Influenced Northern Hemisphere Midlatitudes. *Geophys. Res. Lett.* **2007**, *34*, L13801.

(11) *Clouds; Aerosols Climate Change 2013—The Physical Science Basis; Intergovernmental Panel on Climate Change*; Cambridge University Press: Cambridge, 2014; pp 571−658.

(12) Ramanathan, V.; Crutzen, P. J.; Kiehl, J. T.; Rosenfeld, D. A. Aerosols, Climate, and the Hydrological Cycle. *Science* **2001**, *294*, 2119−2124.

(13) Pope, C. A.; Ezzati, M.; Dockery, D. W. Fine-Particulate Air Pollution and Life Expectancy in the United States. *N. Engl. J. Med.* **2009**, *360*, 376−386.

(14) Calvert, J. G.; Mellouki, A.; Orlando, J. J. *Mechanisms of Atmospheric Oxidation of the Oxygenates*; Oxford University Press: Oxford, New York, 2011.

(15) Calvert, J. G.; Derwent, R. G.; Orlando, J. J.; Wallington, T. J.; Tyndall, G. S. *Mechanisms of Atmospheric Oxidation of the Alkanes*; Oxford University Press: Oxford, New York, 2008.

(16) Kroll, J. H.; Seinfeld, J. H. Chemistry of Secondary Organic Aerosol: Formation and Evolution of Low-Volatility Organics in the Atmosphere. *Atmos. Environ.* **2008**, *42*, 3593−3624.

(17) Vereecken, L.; Aumont, B.; Barnes, I.; Bozzelli, J. W.; Goldman, M. J.; Green, W. H.; Madronich, S.; Mcgillen, M. R.; Mellouki, A.; Orlando, J. J.; et al. Perspective on Mechanism Development and Structure-Activity Relationships for Gas-Phase Atmospheric Chemistry. *Int. J. Chem. Kinet.* **2018**, *50*, 435−469.

(18) Vereecken, L.; Francisco, J. S. Theoretical Studies of Atmospheric Reaction Mechanisms in the Troposphere. *Chem. Soc. Rev.* **2012**, *41*, 6259−6293.

(19) Crounse, J. D.; Nielsen, L. B.; Jørgensen, S.; Kjaergaard, H. G.; Wennberg, P. O. Autoxidation of Organic Compounds in the Atmosphere. *J. Phys. Chem. Lett.* **2013**, *4*, 3513−3520.

(20) Bianchi, F.; Kurtén, T.; Riva, M.; Mohr, C.; Rissanen, M. P.; Roldin, P.; Berndt, T.; Crounse, J. D.; Wennberg, P. O.; Mentel, T. F.; et al. Highly Oxygenated Organic Molecules (HOM) from Gas-Phase Autoxidation Involving Peroxy Radicals: A Key Contributor to Atmospheric Aerosol. *Chem. Rev.* **2019**, *119*, 3472−3509.

(21) Orlando, J. J.; Tyndall, G. S. Laboratory studies of organic peroxy radical chemistry: an overview with emphasis on recent issues of atmospheric significance. *Chem. Soc. Rev.* **2012**, *41*, 6294−6317.

(22) Cox, R. A.; Cole, J. A. Chemical aspects of the autoignition of hydrocarbon—air mixtures. *Combust. Flame* **1985**, *60*, 109−123.

(23) Ingold, K. U. Inhibition of the Autoxidation of Organic Substances in the Liquid Phase. *Chem. Rev.* **1961**, *61*, 563−589.

(24) Hathway, D. E.; Seakins, J. W. T. 300. Autoxidation of Polyphenols. Part III. Autoxidation in Neutral Aqueous Solution of Flavans Related to Catechin. *J. Chem. Soc.* **1957**, 1562−1566.

(25) Angelo, A. J. S.; Vercellotti, J.; Jacks, T.; Legendre, M. Lipid Oxidation in Foods. *Crit. Rev. Food Sci. Nutr.* **1996**, *36*, 175−224.

(26) Perrin, O.; Heiss, A.; Doumenc, F..; Sahetchian, K. Homogeneous and Heterogeneous Reactions of the n-$C_5H_{11}O$, n-$C_5H_{10}OH$ and $OOC_5H_{10}OH$ Radicals in Oxygen. Analytical Steady State Solution by Use of the Laplace Transform. *J. Chem. Soc., Faraday Trans.* **1998**, *94*, 2323−2335.

(27) Jorand, F.; Heiss, A.; Sahetchian, K.; Kerhoas, L.; Einhorn, J. Identification of an Unexpected Peroxide Formed by Successive Isomerization Reactions of the n-Butoxy Radical in Oxygen. *J. Chem. Soc., Faraday Trans.* **1996**, *92*, 4167−4171.

(28) Blin-Simiand, N.; Jorand, F.; Keller, K.; Fiderer, M.; Sahetchian, K. Ketohydroperoxides and Ignition Delay in Internal Combustion Engines. *Combust. Flame* **1998**, *112*, 278−282.

(29) Ehn, M.; Thornton, J. A.; Kleist, E.; Sipilä, M.; Junninen, H.; Pullinen, I.; Springer, M.; Rubach, F.; Tillmann, R.; Lee, B.; et al. A Large Source of Low-Volatility Secondary Organic Aerosol. *Nature* **2014**, *506*, 476−479.

(30) Ehn, M.; Kleist, E.; Junninen, H.; Petäjä, T.; Lönn, G.; Schobesberger, S.; Dal Maso, M.; Trimborn, A.; Kulmala, M.;

Worsnop, D. R.; et al. Gas Phase Formation of Extremely Oxidized Pinene Reaction Products in Chamber and Ambient Air. *Atmos. Chem. Phys.* **2012**, *12*, 5113−5127.
(31) Zhao, J.; Ortega, J.; Chen, M.; McMurry, P.; Smith, J. Dependence of Particle Nucleation and Growth on High Molecular Weight Gas Phase Products during Ozonolysis of α-Pinene. *Atmos. Chem. Phys. Discuss.* **2013**, *13*, 7631−7644.
(32) Jokinen, T.; Sipilä, M.; Richters, S.; Kerminen, V.-M.; Paasonen, P.; Stratmann, F.; Worsnop, D.; Kulmala, M.; Ehn, M.; Herrmann, H.; et al. Rapid Autoxidation Forms Highly Oxidized RO_2 Radicals in the Atmosphere. *Angew. Chem., Int. Ed.* **2014**, *53*, 14596−14600.
(33) Peeters, J.; Müller, J.-F. HO_x radical regeneration in isoprene oxidation via peroxy radical isomerisations. II: experimental evidence and global impact. *Phys. Chem. Chem. Phys.* **2010**, *12*, 14227−14235.
(34) Peeters, J.; Nguyen, T. L.; Vereecken, L. HO_x Radical Regeneration in the Oxidation of Isoprene. *Phys. Chem. Chem. Phys.* **2009**, *11*, 5935.
(35) Da Silva, G.; Graham, C.; Wang, Z.-F. Unimolecular β-Hydroxyperoxy Radical Decomposition with OH Recycling in the Photochemical Oxidation of Isoprene. *Environ. Sci. Technol.* **2010**, *44*, 250−256.
(36) Crounse, J. D.; Paulot, F.; Kjaergaard, H. G.; Wennberg, P. O. Peroxy Radical Isomerization in the Oxidation of Isoprene. *Phys. Chem. Chem. Phys.* **2011**, *13*, 13607−13613.
(37) Praske, E.; Otkjær, R. V.; Crounse, J. D.; Hethcox, J. C.; Stoltz, B. M.; Kjaergaard, H. G.; Wennberg, P. O. Atmospheric Autoxidation Is Increasingly Important in Urban and Suburban North America. *Proc. Natl. Acad. Sci. U.S.A.* **2018**, *115*, 64−69.
(38) Perrin, O.; Heiss, A.; Sahetchian, K.; Kerhoas, L.; Einhorn, J. Determination of the isomerization rate constant $HOCH_2CH_2CH_2CH(OO)CH_3 \rightarrow HOCHCH_2CH_2CH(OOH)CH_3$. Importance of intramolecular hydroperoxy isomerization in tropospheric chemistry. *Int. J. Chem. Kinet.* **1998**, *30*, 875−887.
(39) Vereecken, L.; Nozière, B. H migration in peroxy radicals under atmospheric conditions. *Atmos. Chem. Phys.* **2020**, *20*, 7429−7458.
(40) Vereecken, L.; Müller, J.-F.; Peeters, J. Low-volatility polyoxygenates in the OH-initiated atmospheric oxidation of α-pinene: impact of non-traditional peroxyl radical chemistry. *Phys. Chem. Chem. Phys.* **2007**, *9*, 5241−5248.
(41) Guenther, A.; Karl, T.; Harley, P.; Wiedinmyer, C.; Palmer, P. I.; Geron, C. Estimates of Global Terrestrial Isoprene Emissions Using MEGAN (Model of Emissions of Gases and Aerosols from Nature). *Atmos. Chem. Phys. Discuss.* **2006**, *6*, 3181−3210.
(42) Møller, K. H.; Bates, K. H.; Kjaergaard, H. G. The Importance of Peroxy Radical Hydrogen-Shift Reactions in Atmospheric Isoprene Oxidation. *J. Phys. Chem. A* **2019**, *123*, 920−932.
(43) Paulot, F.; Crounse, J. D.; Kjaergaard, H. G.; Kürten, A.; St. Clair, J. M.; Seinfeld, J. H.; Wennberg, P. O.; Kurten, A.; Clair, St.J. M.; Seinfeld, J. H.; et al. Unexpected Epoxide Formation in the Gas-Phase Photooxidation of Isoprene. *Science* **2009**, *325*, 730−733.
(44) Wennberg, P. O.; Bates, K. H.; Crounse, J. D.; Dodson, L. G.; McVay, R. C.; Mertens, L. A.; Nguyen, T. B.; Praske, E.; Schwantes, R. H.; Smarte, M. D.; et al. Gas-Phase Reactions of Isoprene and Its Major Oxidation Products. *Chem. Rev.* **2018**, *118*, 3337−3390.
(45) Clair, J. M. S.; Crounse, J. D.; Knap, H. C.; Bates, K. H.; Teng, A. P.; Jørgensen, S.; Kjaergaard, H. G.; Keutsch, F. N.; Wennberg, P. O. Kinetics and Products of the Reaction of the First-Generation Isoprene Hydroxy Hydroperoxide (ISOPOOH) with OH. *J. Phys. Chem. A* **2016**, *120*, 1441−1451.
(46) Surratt, J. D.; Kroll, J. H.; Kleindienst, T. E.; Edney, E. O.; Claeys, M.; Sorooshian, A.; Ng, N. L.; Offenberg, J. H.; Lewandowski, M.; Jaoui, M.; et al. Evidence for Organosulfates in Secondary Organic Aerosol. *Environ. Sci. Technol.* **2007**, *41*, 517−527.
(47) Surratt, J. D.; Gómez-González, Y.; Chan, A. W. H.; Vermeylen, R.; Shahgholi, M.; Kleindienst, T. E.; Edney, E. O.; Offenberg, J. H.; Lewandowski, M.; Jaoui, M.; et al. Organosulfate Formation in Biogenic Secondary Organic Aerosol. *J. Phys. Chem. A* **2008**, *112*, 8345−8378.
(48) Paulot, F.; Crounse, J. D.; Kjaergaard, H. G.; Kroll, J. H.; Seinfeld, J. H.; Wennberg, P. O. Isoprene Photooxidation: New Insights into the Production of Acids and Organic Nitrates. *Atmos. Chem. Phys.* **2009**, *9*, 1479−1501.
(49) Surratt, J. D.; Chan, A. W. H.; Eddingsaas, N. C.; Chan, M.; Loza, C. L.; Kwan, A. J.; Hersey, S. P.; Flagan, R. C.; Wennberg, P. O.; Seinfeld, J. H. Reactive Intermediates Revealed in Secondary Organic Aerosol Formation from Isoprene. *Proc. Natl. Acad. Sci. U.S.A.* **2010**, *107*, 6640−6645.
(50) Møller, K. H.; Kurtén, T.; Bates, K. H.; Thornton, J. A.; Kjaergaard, H. G. Thermalized Epoxide Formation in the Atmosphere. *J. Phys. Chem. A* **2019**, *123*, 10620−10630.
(51) D'Ambro, E. L.; Møller, K. H.; Lopez-Hilfiker, F. D.; Schobesberger, S.; Liu, J.; Shilling, J. E.; Lee, B. H.; Kjaergaard, H. G.; Thornton, J. A. Isomerization of Second-Generation Isoprene Peroxy Radicals: Epoxide Formation and Implications for Secondary Organic Aerosol Yields. *Environ. Sci. Technol.* **2017**, *51*, 4978−4987.
(52) Unsleber, J. P.; Reiher, M. The Exploration of Chemical Reaction Networks. *Annu. Rev. Phys. Chem.* **2020**, *71*, 121−142.
(53) Simm, G. N.; Vaucher, A. C.; Reiher, M. Exploration of Reaction Pathways and Chemical Transformation Networks. *J. Phys. Chem. A* **2019**, *123*, 385−399.
(54) Dewyer, A. L.; Argüelles, A. J.; Zimmerman, P. M. Methods for Exploring Reaction Space in Molecular Systems. *Wiley Interdiscip. Rev.: Comput. Mol. Sci.* **2018**, *8*, No. e1354.
(55) Gao, C. W.; Allen, J. W.; Green, W. H.; West, R. H. Reaction Mechanism Generator: Automatic Construction of Chemical Kinetic Mechanisms. *Comput. Phys. Commun.* **2016**, *203*, 212−225.
(56) Liu, M.; Grinberg Dana, A.; Johnson, M. S.; Goldman, M. J.; Jocher, A.; Payne, A. M.; Grambow, C. A.; Han, K.; Yee, N. W.; Mazeau, E. J.; et al. Reaction Mechanism Generator v3.0: Advances in Automatic Mechanism Generation. *J. Chem. Inf. Model.* **2021**, *61*, 2686−2696.
(57) Tyndall, G. S.; Pimentel, A. S.; Orlando, J. J. Temperature Dependence of the Alpha-Ester Rearrangement Reaction. *J. Phys. Chem. A* **2004**, *108*, 6850−6856.
(58) Jenkin, M. E.; Saunders, S. M.; Pilling, M. J. The Tropospheric Degradation of Volatile Organic Compounds: A Protocol for Mechanism Development. *Atmos. Environ.* **1997**, *31*, 81−104.
(59) Saunders, S. M.; Jenkin, M. E.; Derwent, R. G.; Pilling, M. J. Protocol for the Development of the Master Chemical Mechanism, MCM v3 (Part A): Tropospheric Degradation of Non-Aromatic Volatile Organic Compounds. *Atmos. Chem. Phys.* **2003**, *3*, 161−180.
(60) Allen, J. W.; Goldsmith, C. F.; Green, W. H. Automatic Estimation of Pressure-Dependent Rate Coefficients. *Phys. Chem. Chem. Phys.* **2012**, *14*, 1131−1155.
(61) Landrum, G. *RDKit: Open-Source Cheminformatics*. http://www.rdkit.org.
(62) McKinney, W. Pandas: A Foundational Python Library for Data Analysis and Statistics. *Python High Perform. Sci. Comput.* **2011**, *14*, 1−9.
(63) Harris, C. R.; Millman, K. J.; van der Walt, S. J.; Gommers, R.; Virtanen, P.; Cournapeau, D.; Wieser, E.; Taylor, J.; Berg, S.; Smith, N. J.; et al. Array Programming with NumPy. *Nature* **2020**, *585*, 357−362.
(64) Zhu, L.; Johnston, G. Kinetics and Products of the Reaction of the Vinoxy Radical with O2. *J. Phys. Chem.* **1995**, *99*, 15114−15119.
(65) Oguchi, T.; Miyoshi, A.; Koshi, M.; Matsui, H.; Washida, N. Kinetic Study on Reactions of 1-and 2-Methylvinoxy Radicals with O_2. *J. Phys. Chem. A* **2001**, *105*, 378−382.
(66) Delbos, E.; Fittschen, C.; Hippler, H.; Krasteva, N.; Olzmann, M.; Viskolcz, B. Rate Coefficients and Equilibrium Constant for the $CH_2CHO + O_2$ Reaction System. *J. Phys. Chem. A* **2006**, *110*, 3238−3245.
(67) Lelieveld, J.; Butler, T. M.; Crowley, J. N.; Dillon, T. J.; Fischer, H.; Ganzeveld, L.; Harder, H.; Lawrence, M. G.; Martinez, M.; Taraborrelli, D.; et al. Atmospheric Oxidation Capacity Sustained by a Tropical Forest. *Nature* **2008**, *452*, 737−740.

https://doi.org/10.1021/acs.jpca.1c04297
J. Phys. Chem. A 2021, 125, 6772−6788

(68) Berndt, T.; Scholz, W.; Mentler, B.; Fischer, L.; Herrmann, H.; Kulmala, M.; Hansel, A. Accretion Product Formation from Self- and Cross-Reactions of RO_2 Radicals in the Atmosphere. *Angew. Chem., Int. Ed.* **2018**, *57*, 3820−3824.
(69) Orlando, J. J.; Tyndall, G. S.; Wallington, T. J. The Atmospheric Chemistry of Alkoxy Radicals. *Chem. Rev.* **2003**, *103*, 4657−4690.
(70) Otkjær, R. V.; Jakobsen, H. H.; Tram, C. M.; Kjaergaard, H. G. Calculated Hydrogen Shift Rate Constants in Substituted Alkyl Peroxy Radicals. *J. Phys. Chem. A* **2018**, *122*, 8665−8673.
(71) Chen, J.; Møller, K. H.; Wennberg, P. O.; Kjaergaard, H. G. Unimolecular Reactions Following Indoor and Outdoor Limonene Ozonolysis. *J. Phys. Chem. A* **2021**, *125*, 669−680.
(72) DeSain, J. D.; Taatjes, C. A.; Miller, J. A.; Klippenstein, S. J.; Hahn, D. K. Infrared Frequency-Modulation Probing of Product Formation in Alkyl + O_2 Reactions. Part IV. Reactions of Propyl and Butyl Radicals with O_2. *Faraday Discuss.* **2002**, *119*, 101−120.
(73) Villano, S. M.; Huynh, L. K.; Carstensen, H.-H.; Dean, A. M. High-Pressure Rate Rules for Alkyl + O_2 Reactions. 2. The Isomerization, Cyclic Ether Formation, and β-Scission Reactions of Hydroperoxy Alkyl Radicals. *J. Phys. Chem. A* **2012**, *116*, 5068−5089.
(74) Wijaya, C. D.; Sumathi, R.; Green, W. H. Thermodynamic Properties and Kinetic Parameters for Cyclic Ether Formation from Hydroperoxyalkyl Radicals. *J. Phys. Chem. A* **2003**, *107*, 4908−4920.
(75) Bugler, J.; Power, J.; Curran, H. J. A Theoretical Study of Cyclic Ether Formation Reactions. *Proc. Combust. Inst.* **2017**, *36*, 161−167.
(76) Bloodworth, A. J.; Davies, A. G.; Griffin, I. M.; Muggleton, B.; Roberts, B. P. Rate Constants for the Formation of Oxiranes from β-Peroxyalkyl Radicals. Gem-Dialkyl Effect in Homolytic Ring Closure. *J. Am. Chem. Soc.* **1974**, *96*, 7599−7601.
(77) Chan, W.-T.; Pritchard, H. O.; Hamilton, I. P. Dissociative Ring-Closure in Aliphatic Hydroperoxyl Radicals. *Phys. Chem. Chem. Phys.* **1999**, *1*, 3715−3719.
(78) Wu, D.; Bayes, K. D. Rate Constants for the Reactions of Isobutyl, Neopentyl, Cyclopentyl, and Cyclohexyl Radicals with Molecular Oxygen. *Int. J. Chem. Kinet.* **1986**, *18*, 547−554.
(79) Atkinson, R. Gas-Phase Tropospheric Chemistry of Volatile Organic Compounds: 1. Alkanes and Alkenes. *J. Phys. Chem. Ref. Data* **1997**, *26*, 215−290.
(80) Knox, J. H.; Kinnear, C. G. The mechanism of combustion of pentane in the gas phase between 250° and 400°C. *Symp. (Int.) Combust.* **1971**, *13*, 217−227.
(81) Baldwin, R. R.; Hisham, M. W. M.; Walker, R. W. Arrhenius Parameters of Elementary Reactions Involved in the Oxidation of Neopentane. *J. Chem. Soc., Faraday Trans. 1* **1982**, *78*, 1615−1627.
(82) Vereecken, L. Reaction Mechanisms for the Atmospheric Oxidation of Monocyclic Aromatic Compounds. *Advances in Atmospheric Chemistry*; World Scientific, 2019; pp 377−527.
(83) Birdsall, A. W.; Andreoni, J. F.; Elrod, M. J. Investigation of the Role of Bicyclic Peroxy Radicals in the Oxidation Mechanism of Toluene. *J. Phys. Chem. A* **2010**, *114*, 10655−10663.
(84) Lay, T. H.; Bozzelli, J. W.; Seinfeld, J. H. Atmospheric Photochemical Oxidation of Benzene: Benzene + OH and the Benzene−OH Adduct (Hydroxyl-2,4-cyclohexadienyl) + O2. *J. Phys. Chem.* **1996**, *100*, 6543−6554.
(85) Ma, F.; Guo, X.; Xia, D.; Xie, H.-B.; Wang, Y.; Elm, J.; Chen, J.; Niu, J. Atmospheric Chemistry of Allylic Radicals from Isoprene: A Successive Cyclization-Driven Autoxidation Mechanism. *Environ. Sci. Technol.* **2021**, *55*, 4399−4409.
(86) Richters, S.; Pfeifle, M.; Olzmann, M.; Berndt, T. Endo-Cyclization of Unsaturated RO_2 Radicals from the Gas-Phase Ozonolysis of Cyclohexadienes. *Chem. Commun.* **2017**, *53*, 4132−4135.
(87) Roe, A. N.; McPhail, A. T.; Porter, N. A. Serial Cyclization: Studies in the Mechanism and Stereochemistry of Peroxy Radical Cyclization. *J. Am. Chem. Soc.* **1983**, *105*, 1199−1203.
(88) Møller, K. H.; Otkjær, R. V.; Chen, J.; Kjaergaard, H. G. Double Bonds Are Key to Fast Unimolecular Reactivity in First-Generation Monoterpene Hydroxy Peroxy Radicals. *J. Phys. Chem. A* **2020**, *124*, 2885−2896.
(89) Vereecken, L.; Peeters, J. Nontraditional (Per)Oxy Ring-Closure Paths in the Atmospheric Oxidation of Isoprene and Monoterpenes. *J. Phys. Chem. A* **2004**, *108*, 5197−5204.
(90) Sebbar, N.; Bozzelli, J. W.; Trimis, D.; Bockhorn, H. Thermochemistry and kinetics of the 2-butanone-4-yl $CH_3C(=O)$-CH_2CH_2 + O_2 reaction system. *Int. J. Chem. Kinet.* **2019**, *51*, 541−562.
(91) Atkinson, R. Rate constants for the atmospheric reactions of alkoxy radicals: An updated estimation method. *Atmos. Environ.* **2007**, *41*, 8468−8485.
(92) Yamabe, S.; Tsuchida, N.; Miyajima, K. Reaction Paths of Keto−Enol Tautomerization of β-Diketones. *J. Phys. Chem. A* **2004**, *108*, 2750−2757.

https://doi.org/10.1021/acs.jpca.1c04297
J. Phys. Chem. A 2021, 125, 6772−6788